Univerzita Karlova v Praze
Matematicko-fyzikální fakulta

DIPLOMOVÁ PRÁCE

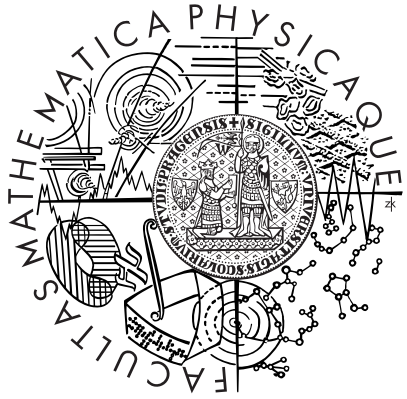

Jan Olšina

Přenos koherencí při relaxaci excitační energie v molekulárních agregátech

Ústav teoretické fyziky

Vedoucí diplomové práce: RNDr. Tomáš Mančal, Ph.D.,
Studijní program: fyzika, teoretická fyzika

2009

Charles University in Prague
Faculty of Mathematics and Physics

DIPLOMA THESIS

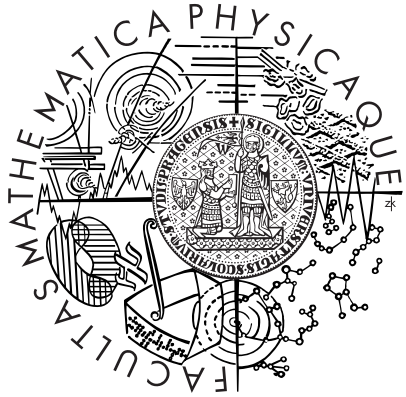

Jan Olšina

Coherence Transfer During Relaxation in Molecular Aggregates

Institute of Theoretical Physics

Supervisor: RNDr. Tomáš Mančal, Ph.D.

Study programme: physics, theoretical physics

2009

Tímto děkuji RNDr. Tomáši Mančalovi, Ph.D. za cenné a trpělivé konzultace a rady, bez kterých by tato práce nemohla vzniknout. Poděkování patří též mým rodičům, kteří mě podporovali po celou dobu studia.

Prohlašuji, že jsem svou diplomovou práci napsal samostatně a výhradně s použitím citovaných pramenů. Souhlasím se zapůjčováním práce a jejím zveřejňováním.

V Praze dne 16.4.2009 Jan Olšina

Contents

Abstract **v**

Introduction **1**
Notation . . . 2
Spectroscopic Units . . . 3

1 Used Theory **4**
1.1 Brief Summary of the Density Operator Formalism . . . 4
1.2 Superoperator Representation . . . 5
1.3 Superoperator Projectors . . . 6
1.4 Quantum Master Equation . . . 6
1.4.1 Definitions . . . 6
1.4.2 QME Derivation . . . 7
1.5 Correlation Functions . . . 9
1.5.1 Correlation Function and Thermodynamics . . . 9
1.5.2 Correlation Function of a Damped Harmonic Oscillator . . . 11
1.6 Markov Approximation . . . 12
1.7 Secular Approximation . . . 13
1.8 Thermodynamic Equilibrium . . . 13
1.9 Fourier Transform Solution of the QME . . . 14
1.9.1 Discrete Fourier Transform . . . 15
1.9.2 Numerical Handling of the Regularization . . . 16
1.9.3 Convergence of the DFT . . . 16
1.10 Initial Conditions Created by an Ultra-Short Laser Pulse . . . 18

2 System Model **20**
2.1 Hamiltonian . . . 20
2.1.1 Monomer Hamiltonian . . . 20
2.1.2 Aggregate Hamiltonian . . . 22
2.2 Correlation Functions . . . 23
2.3 Asymptotic Behaviour of a Markov Approximation-Based Algorithm . . . 24
2.4 Direct Solution of the QME by Expanding Correlation Functions into Exponential Functions . . . 24

3 Results of Numerical Computation **26**
3.1 Failure of the Markov Approximation with Non-Secular Terms 26
3.1.1 Markov Approximation Failure in Case of a Dimer 27
3.2 Numerical Instability in Direct Solution of the QME 28
3.3 Discussion of Canonical Equilibrium in the QME 28
3.4 Time Evolution of a Trimer 30
3.4.1 Parameters of the Numerical Experiment 30
3.4.2 Comparison of the Time Evolution in Various Approximations . . . 31
3.4.3 Temperature Dependence 32
3.4.4 Coherence Transfer Effects, Time Evolution Superoperator 32

4 Conclusion **34**

A Supplementary Graphs **36**
A.1 Comparison of Evaluation Methods, Trimer 37
A.2 Trimer Time-Evolution Superoperator 42
A.3 Temperature Dependence, Trimer 47
A.4 Trimer Time Evolution for Another Interesting Cases 49

Bibliography **51**

Název práce: Přenos koherencí při relaxaci excitační energie v molekulárních agregátech
Autor: Jan Olšina
Katedra (ústav): Ústav teoretické fyziky
Vedoucí diplomové práce: RNDr. Tomáš Mančal, Ph.D.
e-mail vedoucího: mancal@karlov.mff.cuni.cz

Abstrakt: Předložená práce zkoumá časový vývoj operátoru hustoty agregátů molekul v interakci s termodynamickou lázní s účelem najít vhodnou aproximaci pro popis vlivu přenosu koherencí na tento vývoj. Opírá se o výsledky autorem sestaveného programu pro výpočet vývoje třemi metodami – řešením konvoluční Quantum Master Equation a řešení z ní odvozených Redfieldových rovnic v Markovské aproximaci a následné Sekulární aproximaci. Na základě prezentovaných numerických výsledků programu, na příkladu trimeru, byla zkoumána teplotní závislost řešení a jeho závislost na některých dalších parametrech modelu a vliv přenosu koherencí na dílčí komponenty evolučního superoperátoru. V práci je rovněž odůvodněno, proč Markovská aproximace selhává pro široký rozsah parametrů a není proto vhodná pro popis problematiky přenosu koherencí.
Klíčová slova: přenos koherencí, časový vývoj, otevřené kvantové systémy, agregáty molekul

Title: Coherence Transfer During Relaxation in Molecular Aggregates
Author: Jan Olšina
Department: Institute of Theoretical Physics
Supervisor: RNDr. Tomáš Mančal, Ph.D.
Supervisor's e-mail address: mancal@karlov.mff.cuni.cz

Abstract: We study the time dependence of the density operator of molecular aggregates in contact with thermal bath, to find a proper approximation for the description of a coherence transfer influence on this evolution. It is based on results of the computer program, written by the author of the work. The program uses three methods of evaluation – the solution of the convolution Quantum Master Equation, and solution of the derived Redfield equations in Markov and subsequent Secular approximations. The temperature dependence and dependence on other parameters of the model are discussed on the basis of the obtained numerical results performed on an example of a trimer. The influence of coherence transfer on time-evolution superoperator of the trimer is discussed as well. The reasons why the Markov approximation fails for a wide spectrum of parameters are given. It is concluded that it is not suitable for the description of coherence transfer effects.
Keywords: coherence transfer, time evolution, open quantum systems, molecular aggregates

Introduction

Small molecules often form functional aggregates in Nature. This is particularly important in biophysics, where molecular aggregates play an important role in many processes. For example in photosynthesis, chloroplast pigment molecules bunch into so called light-harvesting photosynthetic antennae [1]. This enables the cell to catch light more efficiently, because the antenna has larger effective cross-section than the pigment molecule itself. Energy is transferred into so called reaction centers on various time scales after that.

An ultrafast time evolution of electronic states of such molecular aggregates is a subject of experimental studies by means of a femtosecond optical spectroscopy – pump-probe, hole-burning, two dimensional spectroscopy [2], and other methods. This is connected with the studies of energy transfer in biological systems [3]. Ultrafast energy transfer has been observed in LHC-II [4] and in Fenna-Matthews-Olson bacteriochlorophyll *a* protein (FMO) complexes in the Green bacterium [3], and many other photosynthetic systems.

Theoreticians are focused particularly on 2D femtosecond spectroscopy recently, (see e.g. [2] for more details), because it enables to investigate not only the time evolution of the aggregate populations of states, but also the time evolution of coherences between them. It opens a unique possibility for testing variety of models and comparing them with experimental data, such as Engel's and Fleming's measurement on the FMO[1] [5].

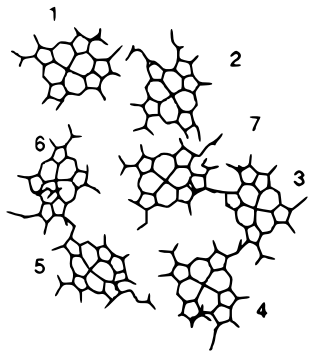

Figure 1: Structure of the FMO complex, [1].

[1]The FMO protein was the first chlorophyll-containing protein to have its structure determined to atomic resolution. For this reason, much of a current understanding of the principles of pigment-protein derives from studies of this system [1]. These results make it interesting for further investigation.

To calculate a spectroscopic response for the above mentioned molecular aggregate models, we need to consider the system time evolution. Since the investigated molecular aggregates are not isolated systems, Schrödinger equation is not applicable and another description has to be used. The Quantum Master Equation (QME), which can be derived by the Nakajima-Zwanzig formalism [6, 7], is widely used for that purpose. It is based on an often well-founded approximations (see Ref. [6]), particularly that surrounding of the system can be described statistically and part of density operator describing it can be projected out. Since the QME is an integro-differential equation and therefore not simple for numerical solution, additional approximations are often used, namely the Markov approximation and subsequent secular approximation. Using these, the QME can be converted into an ordinary differential equation.

Both of these approximations have some problems – the Markov approximation, as we show in this work, breaks down for wide range of parameters and leads to completely unphysical thermodynamic equilibrium in these cases. The secular approximation can fix this problem, but completely neglects the coherence transfer terms. There are articles [8, 9] suggesting coherence transfer effects are generally negligible and the secular approximation gives accurate description of the open system evolution, but also papers against [10].

In this work, we apply the above mentioned formalism to molecular aggregates, which we describe by a simple model. We investigate the question whether the coherence transfer effects play important role in system evolution, how strong these effects are, and how much do the above mentioned approximations differ from the QME. Our concern in the coherence transfer is motivated by measurements performed on FMO complex. They show that there are oscillations in FMO 2D spectrum lasting so long, that it cannot be explained by the secular Redfield theory [5]. This indicates that the coherence transfer terms, best described by the QME without the additional approximations, could be responsible for these oscillations. We compare the QME with the Markov and the secular approximations in this work. We illustrate, that the QME is the best of these methods for coherence transfer description on an example of a trimer. We subsequently calculate its evolution superoperator components to study coherence transfer.

Notation

In this work we use the common bra-ket formalism. Operators defined on system's Hilbert space are denoted by a hat-symbol as $\hat{O}$. The density operator is denoted by letter ρ, without hat. Superoperators, expressing general linear action on the density operator, are denoted like $\mathcal{O}$. If we explicitly write matrix indices, they always go through the states of the system. Lower indices denote matrix element in given representation while upper indices refer to the matrix/operator itself. (They are used e.g. for labelling of projector operators, etc.) The Einstein summation rule is not used. All summations are denoted explicitly. A^+ denotes a matrix hermitian conjugate to a matrix A, A^* stands for a complex conjugate matrix and A^{T} is a transposed matrix, but we use more often explicit index notation for matrix transpose. Bachmann-Landau symbol ("Big Oh" symbol), used for notation of

algorithm asymptotic behaviour, is denoted $\mathrm{O}(f(n))$. (We do not use standard $\mathcal{O}$-notation since it conflicts with the superoperator notation). In whole work, we use the following convention and notation for the Fourier transform:

$$\tilde{f}(\omega) = \int_{-\infty}^{\infty} dt\, f(t)\, e^{-it\omega} \,, \tag{1a}$$

$$f(t) = \frac{1}{2\pi} \int_{-\infty}^{\infty} d\omega\, \tilde{f}(\omega)\, e^{it\omega} \,. \tag{1b}$$

Spectroscopic Units

We use the widely used "spectroscopic" units in this work. Distance is measured in Ångströms, temperature in Kelvins, time in femtoseconds and energy is given by wavenumber of a photon with given energy

$$E = h\nu = 2\pi\hbar\frac{c}{\lambda} = 2\pi\hbar c k \,. \tag{2}$$

Here, λ denotes the wavelength, k represents the wavenumber, c is the speed of light and $\hbar$ denotes the reduced Planck's constant. We are free to set values of $\hbar$ and c, because they just scale our units to natural units. In spectroscopic units, we require

$$2\pi\hbar c = 1 \,. \tag{3}$$

Considering

$$\begin{aligned}
\hbar &= 1.05457 \times 10^{-34}\ \mathrm{m^2\,kg\,s^{-1}} \,, \\
c &= 2.99792458 \times 10^{8}\ \mathrm{m\,s^{-1}} \,, \\
k_\mathrm{B} &= 1.3806503 \times 10^{-23}\ \mathrm{m^2\,kg\,s^{-2}\,K^{-1}} \,,
\end{aligned}$$

we get

$$2\pi\hbar c = 1.98645 \times 10^{-23}\ \mathrm{J/cm^{-1}} \,,$$

therefore

$$\begin{aligned}
\mathrm{J} &= 5.03412 \times 10^{22}\ \mathrm{cm^{-1}} \,, \\
\hbar &= 5308.84\ \mathrm{fs\,cm^{-1}} \,, \\
c &= 2.99792 \times 10^{-5}\ \mathrm{fs^{-1}\,cm} \,, \\
k_\mathrm{B} &= 0.695036\ \mathrm{cm^{-1}\,K^{-1}} \,.
\end{aligned}$$

In these units, most of results are stated, but for the numerical calculation it is more proper to use units, in which the above mentioned basic constants are approximately equal to 1.

Chapter 1

Used Theory

1.1 Brief Summary of the Density Operator Formalism

When we study an open quantum system, which is surrounded by a greater system (reservoir), we encounter the problem, that unless the systems are non-interacting at all, the total wave function $\Psi(s_i, r_j)$, where s_i are variables related to the system and r_j to the reservoir, cannot be separated into $\psi_{\mathrm{S}}(s_i)\psi_{\mathrm{R}}(r_j)$. Furthermore it is impossible to describe the subsystem by a wave function $\psi_{\mathrm{S}}(s_i)$, where the variables r_j have been projected out. As an example let's consider two electrons which have been prepared in a state

$$|\Psi\rangle = |\uparrow\rangle\,|\uparrow\rangle + |\downarrow\rangle\,|\downarrow\rangle \ . \tag{1.1}$$

The first electron cannot be clearly described by a one-electron wave function – if we choose any linear combination of states $|\uparrow\rangle$, $|\downarrow\rangle$, there would have to be a proper basis in which the electron was in a pure state. However this is not possible – information about the electron state is encoded in the state of the second electron and therefore we cannot recognize its state from statistical ensemble of electrons in states $|\uparrow\rangle$, $|\downarrow\rangle$, with no superposition through any measurement, done only on the first electron. Such states are called mixed states and we need the density operator formalism to describe them. (One can read more on this topic in Ref. [6, 7].)

In density operator formalism, system state is fully described by an operator ρ, (expressed by matrix elements ρ_{ij}), which determines statistical behaviour of the system. In case of statistical ensemble, the density operator is defined as

$$\rho = \sum_i \omega_i\,|\Psi_i\rangle\,\langle\Psi_i|\,, \tag{1.2}$$

where ω_i are probabilities of occupancy of i-th pure state. Density matrix formalism cannot distinguish between statistical ensemble of systems in pure states, where ω_i describes probability of getting the system in state $|i\rangle$ and between statistical ensemble of (all the

same) systems in states similar to the state from Eq. (1.1). One might argue that there is even no difference between them, because statistical ensemble was prepared, just like the state from Eq. (1.1), by entanglement with a greater system – the measuring instrument. We called states (1.2) *mixed states*.

Density matrix has trace normalized to unity $\mathrm{Tr}\,\rho = 1$. Mean value of a physical quantity represented by an operator $\hat{A}$ is given by

$$\left\langle \hat{A} \right\rangle = \mathrm{Tr}\,\hat{A}\rho. \tag{1.3}$$

Probabilities of finding the system in a given state in chosen basis are given by diagonal elements of density matrix. The time evolution of system is given by Liouville equation

$$\frac{\partial \rho}{\partial t} = -\frac{i}{\hbar}\left[\hat{H}, \rho\right]_- \ , \tag{1.4}$$

which can be easily derived from Schrödinger equation.

1.2 Superoperator Representation

In the density operator formalism, action of a general linear operator on the system cannot be described as an action of a matrix on a vector, because ρ is not vector of system Hilbert space. It is therefore convenient to introduce "superoperator representation", in which we write action of a superoperator as

$$(\mathcal{A}\rho)_{mn} = \sum_{m'n'} \mathcal{A}_{mn,m'n'}\rho_{m'n'}. \tag{1.5}$$

Comma denotes that we consider pair of indices to form one multiindex in superoperator representation. We define superoperator Kronecker δ as

$$\delta_{ij,i'j'} \equiv \delta_{ii'}\delta_{jj'}. \tag{1.6}$$

Which representation is currently used in text can be easily found out by index structure of particular formula. In superoperator notation, Liouville equation (1.4) takes form of

$$\frac{d}{dt}\rho(t) = -i\mathcal{L}\rho(t) \ , \tag{1.7}$$

where

$$\mathcal{L}\bullet \equiv \frac{1}{\hbar}\left[\hat{H}, \bullet\right]_- \tag{1.8}$$

is the so-called Liouville superoperator or Liouvillian.

1.3 Superoperator Projectors

Let us denote the projector on a s-th state by $\hat{P}_s$. It is defined as

$$\left(\hat{P}_s\right)_{ij} \equiv \delta_{is}\delta_{js}. \tag{1.9}$$

We introduce projector on ij,kl-th component of superoperator $\mathcal{P}^{ij,kl}$ as

$$\left(\mathcal{P}^{ij,kl}\mathcal{O}\right)_{i'j',k'l'} \equiv \mathcal{O}_{ij,kl}\,\delta_{ij,i'j'}\,\delta_{kl,k'l'}\,. \tag{1.10}$$

Let us explicitly highlight that Einstein summation rule is not used here. We easily verify that relation

$$\mathcal{P}^2 = \mathcal{P} \tag{1.11}$$

holds.

For superoperators whose action on density matrix has a form of a product of two general matrices from right and left

$$\mathcal{O}\rho = \hat{O}^{\mathrm{l}}\rho\hat{O}^{\mathrm{r}} \tag{1.12}$$

we can write $\mathcal{P}_{ij,kl}$ as

$$\mathcal{P}^{ij,kl}\mathcal{O} = \hat{P}_i\hat{O}^{\mathrm{l}}\hat{P}_k\rho\,\hat{P}_l\hat{O}^{\mathrm{r}}\hat{P}_j\,. \tag{1.13}$$

Relation (1.11) is evidently satisfied here since Eq. (1.13) has again a form of Eq. (1.12) and $\hat{P}_i$ are projectors.

Of course not all superoperators have a form of Eq. (1.12) since the number of elements of a general superoperator is N^4 (where N is the size of the basis of the used Hilbert space), while each of matrices $\hat{O}^{\mathrm{l}}$, $\hat{O}^{\mathrm{r}}$ have only N^2 elements. However, all superoperators used here can be expressed by the Eq. (1.13), or as sum of such terms.

1.4 Quantum Master Equation

There is an apparatus for modelling the time evolution of open systems based on several assumptions. We will briefly repeat derivation of the Quantum Master Equation, following [6], and discuss which approximation we make and how well they are satisfied.

1.4.1 Definitions

Let us write the complete Hamiltonian of a quantum system as

$$\hat{H} = \hat{H}_{\mathrm{S}} + \hat{H}_{\mathrm{S-R}} + \hat{H}_{\mathrm{R}}\,, \tag{1.14}$$

where $\hat{H}_{\mathrm{S}}$, $\hat{H}_{\mathrm{R}}$ act only on the subsystem, reservoir respectively. The operator $\hat{H}_{\mathrm{S-R}}$ present the interaction between the subsystem and the reservoir. Now we introduce interaction representation. Let

$$\hat{U}_{\mathrm{S}}(t) = e^{-\frac{i}{\hbar}\hat{H}_{\mathrm{S}}t} \tag{1.15}$$

be time evolution operator of the unperturbed system. Then a given operator $\hat{A}$ in interaction representation is

$$\hat{A}^{(\mathrm{I})} = \hat{U}_{\mathrm{S}}^{+}\hat{A}\hat{U}_{\mathrm{S}} \,. \tag{1.16}$$

We furthermore define projectors

$$\mathcal{P}\bullet \equiv \rho_{\mathrm{R}}\mathrm{Tr}_{\mathrm{R}}\bullet \,, \tag{1.17}$$

$$\mathcal{Q} \equiv 1 - \mathcal{P} \tag{1.18}$$

in order to separate subsystem and reservoir parts of the complete density operator $\rho_{\mathrm{S+R}}$. Property (1.11) holds since $\mathrm{Tr}_{\mathrm{R}}\rho_{\mathrm{R}} = 1$ and ρ_{R} acts only on reservoir states.

The basis of the used Hilbert space in which $\hat{H}_{\mathrm{S}}$ is diagonal, so-called *exciton basis*, has a special importance. On one hand, it is because in the canonical thermodynamic equilibrium, into which a *closed* system finally evolves, the density matrix (1.25) is diagonal particularly in the exciton basis. Therefore it is almost the right basis for description of the thermal equilibrium of open systems, if the system-reservoir coupling is small. On the other hand, because any spectroscopic measurement on the system projects it to $\hat{H}_{\mathrm{S}}$ energy eigenstate, in the exciton basis. We denote operators and superoperators in exciton basis by superscript $\hat{A}^{(\mathrm{exc})}$.

1.4.2 QME Derivation

We begin with the density matrix of the whole system $\rho_{\mathrm{S+R}}(t)$. Its time evolution is governed by the Liouville equation

$$\frac{d}{dt}\rho_{\mathrm{S+R}}(t) = -\frac{i}{\hbar}\left[\hat{H}, \rho_{\mathrm{S+R}}(t)\right]_{-} \,. \tag{1.19}$$

Now assume that our system is composed of a small subsystem, an open system whose time evolution we want to model, and its surrounding (reservoir), which is in good approximation in thermal equilibrium. We are interested in time evolution of the subsystem reduced density matrix

$$\rho_{\mathrm{S}}(t) = \mathrm{Tr}_{\mathrm{R}}\left(\rho_{\mathrm{S+R}}(t)\right), \tag{1.20}$$

while the reservoir is described only statistically. Tr_{R} traces through reservoir states of the system.

Let us take, following Ref. [6], trace of Eq. (1.19) over reservoir states. We receive

$$\begin{aligned}\frac{d}{dt}\rho_{\mathrm{S}}(t) &= -\frac{i}{\hbar}\mathrm{Tr}_{\mathrm{R}}\left[\hat{H}_{\mathrm{S}}+\hat{H}_{\mathrm{S-R}}+\hat{H}_{\mathrm{R}},\rho_{\mathrm{S+R}}(t)\right]_{-} \\ &= -\frac{i}{\hbar}\left[\hat{H}_{\mathrm{S}},\rho_{\mathrm{S}}(t)\right]_{-} - \frac{i}{\hbar}\mathrm{Tr}_{\mathrm{R}}\left[\hat{H}_{\mathrm{S-R}}+\hat{H}_{\mathrm{R}},\rho_{\mathrm{S+R}}(t)\right]_{-} . \end{aligned} \tag{1.21}$$

Because of cyclic invariance of trace and the fact that $\hat{H}_{\mathrm{R}}$ acts purely on the reservoir states of the system commutator of $\hat{H}_{\mathrm{R}}$ and $\rho_{\mathrm{S+R}}(t)$ vanishes.

Let us assume $\hat{H}_{\mathrm{S-R}}$ to be in the form

$$\hat{H}_{\mathrm{S-R}} = \sum_{u}\hat{P}_{u}\Phi_{u} , \tag{1.22}$$

where $\hat{P}_u$ acts solely on the subsystem states and Φ_u solely on the reservoir states. There are good physical reasons for this separation and it is self-consistent with our system model, described in the Chapter 2. See Eq. (2.4).

After introducing *mean-field approximation*, i.e. replacing $\hat{H}_{\mathrm{S-R}}$ by expectation value of the result, Eq. (1.21) splits into two

$$\frac{d}{dt}\rho_{\mathrm{S}}(t) = -\frac{i}{\hbar}\left[\hat{H}_{\mathrm{S}}+\sum_{u}\hat{P}_{u}\mathrm{Tr}_{\mathrm{R}}\left(\Phi_{u}\rho_{\mathrm{R}}(t)\right),\rho_{\mathrm{S}}\right] \tag{1.23a}$$

$$\frac{d}{dt}\rho_{\mathrm{R}}(t) = -\frac{i}{\hbar}\left[\hat{H}_{\mathrm{R}}+\sum_{u}\Phi_{u}\mathrm{Tr}_{\mathrm{S}}\left(\hat{P}_{u}\rho_{\mathrm{S}}(t)\right),\rho_{\mathrm{R}}\right] . \tag{1.23b}$$

As shown in Ref. [6], applying the second order perturbation theory on equation (1.23a) in the interaction picture, we can write

$$\begin{aligned}\frac{d}{dt}\rho_{\mathrm{S}}^{(\mathrm{I})}(t) =& -\frac{i}{\hbar}\mathrm{Tr}_{\mathrm{R}}\left(\rho_{\mathrm{R}}^{\mathrm{eq}}\left[\hat{H}_{\mathrm{S-R}}^{(\mathrm{I})}(t),\rho_{\mathrm{S}}^{(\mathrm{I})}(t)\right]_{-}\right) \\ &-\frac{1}{\hbar^{2}}\int_{t_0}^{t}d\tau\,\mathrm{Tr}_{\mathrm{R}}\left(\left[\hat{H}_{\mathrm{S-R}}^{(\mathrm{I})}(t),(1-\mathcal{P})\left[\hat{H}_{\mathrm{S-R}}^{(\mathrm{I})}(\tau),\rho_{\mathrm{R}}^{\mathrm{eq}}\rho_{\mathrm{S}}^{(\mathrm{I})}(\tau)\right]_{-}\right]_{-}\right) ,\end{aligned} \tag{1.24}$$

where

$$\rho_{\mathrm{R}}^{\mathrm{eq}} = \frac{e^{-\frac{\hat{H}_{\mathrm{R}}}{k_{\mathrm{B}}T}}}{\mathrm{Tr}_{\mathrm{R}}\left(e^{-\frac{\hat{H}_{\mathrm{R}}}{k_{\mathrm{B}}T}}\right)} , \tag{1.25}$$

and $\rho_{\mathrm{R}} = \rho_{\mathrm{R}}^{\mathrm{eq}}$ in the projector (1.17). Now we replace Φ_u by its mean values and fluctuations from mean values using statistical description of reservoir. We define correlation functions as

$$C_{uv}(t) = \frac{1}{\hbar^{2}}\left\langle\Delta\Phi_{u}(t)\Delta\Phi_{v}(0)\right\rangle_{\mathrm{R}} , \tag{1.26}$$

where

$$\Delta\Phi_u(t) = \Phi_u(t) - \langle\Phi_u\rangle_{\mathrm{R}} \ , \tag{1.27}$$

$$\langle\bullet\rangle_{\mathrm{R}} \equiv \mathrm{Tr}_{\mathrm{R}}(\bullet) \ . \tag{1.28}$$

Considering this, equation (1.24) takes form

$$\begin{aligned}\frac{d}{dt}\rho_{\mathrm{S}}^{(\mathrm{I})}(t) = &-\frac{i}{\hbar}\sum_u \langle\Phi_u\rangle \left[\hat{P}_u^{(\mathrm{I})}(t), \rho_{\mathrm{S}}^{(\mathrm{I})}(t)\right]_- \\ &-\sum_{uv}\int_{t_0}^{t} d\tau \left(C_{uv}(t-\tau)\left[\hat{P}_u^{(\mathrm{I})}(t), \hat{P}_v^{(\mathrm{I})}(\tau)\rho_{\mathrm{S}}^{(\mathrm{I})}(\tau)\right]_- \right. \\ &\left. -C_{uv}(-t+\tau)\left[\hat{P}_u^{(\mathrm{I})}(t), \rho_{\mathrm{S}}^{(\mathrm{I})}(\tau)\hat{P}_v^{(\mathrm{I})}(\tau)\right]_- \right) \ .\end{aligned} \tag{1.29}$$

This is the well known *Quantum Master Equation*. How is the system affected by reservoir depends on a particular form of the correlation function.

It can be shown [6] that Eq. (1.29) takes form

$$\begin{aligned}\frac{d}{dt}\rho_{\mathrm{S}}(t) = &-\frac{i}{\hbar}\left[\hat{H}_{\mathrm{S}} + \sum_u \langle\Phi_u\rangle \hat{P}_u, \rho_{\mathrm{S}}(t)\right]_- \\ &-\sum_{uv}\int_{t_0}^{t} d\tau \left(C_{uv}(\tau)\left[\hat{P}_u, \hat{U}_{\mathrm{S}}(\tau)\hat{P}_v\rho_{\mathrm{S}}(t-\tau)\hat{U}_{\mathrm{S}}^{+}(\tau)\right]_- \right. \\ &\left. -C_{uv}(-\tau)\left[\hat{P}_u, \hat{U}_{\mathrm{S}}(\tau)\rho_{\mathrm{S}}(t-\tau)\hat{P}_v\hat{U}_{\mathrm{S}}^{+}(\tau)\right]_- \right) \ .\end{aligned} \tag{1.30}$$

in Schrödinger picture.

1.5 Correlation Functions

1.5.1 Correlation Function and Thermodynamics

In the previous section, we have seen that in the second order perturbation theory, the information about the evolution of the reservoir, including its thermodynamical properties, is contained in correlation functions (1.26). We will specify a particular form of the correlation functions later. Let us now investigate, which properties can be derived generally from the thermodynamics.

As discussed in Ref. [6], one can derive that all correlation functions fulfil property

$$C_{uv}(t) = \frac{1}{\hbar^2}\langle\Delta\Phi_u(t)\Delta\Phi_v(0)\rangle_{\mathrm{R}} = \left[\frac{1}{\hbar^2}\langle\Delta\Phi_v(0)\Delta\Phi_u(t)\rangle_{\mathrm{R}}\right]^* = C_{vu}^*(-t) \ , \tag{1.31}$$

or

$$\tilde{C}^*_{uv}(\omega) = \tilde{C}_{vu}(\omega), \tag{1.32}$$

where

$$\tilde{C}_{uv}(\omega) \equiv \int dt\; e^{-i\omega t} C_{uv}(t). \tag{1.33}$$

There is another important property of the correlation functions, relating it to the temperature of the bath. Let us start denoting its real and imaginary part

$$C^{(+)}_{uv}(t) = C_{uv}(t) + C^*_{uv}(t), \qquad C^{(-)}_{uv}(t) = C_{uv}(t) - C^*_{uv}(t)\;. \tag{1.34}$$

Now if we take into account the definition (1.26), we can rewrite Eq. (1.33) as

$$\begin{aligned}\tilde{C}_{uv}(\omega) =& \frac{1}{\hbar^2}\int dt\; e^{-i\omega t}\sum_{\alpha\beta}\langle\alpha|\,\rho^{\rm eq}_{\rm R} e^{i\hat{H}_{\rm R}t/\hbar}\Delta\Phi_u e^{-i\hat{H}_{\rm R}t/\hbar}\,|\beta\rangle\,\langle\beta|\,\Delta\Phi_v\,|\alpha\rangle \\ =& \frac{1}{\hbar^2}\sum_{\alpha\beta}\int dt\; e^{-i(\omega+\omega_{\alpha\beta})t} f(E_\beta)\,\langle\beta|\,\Delta\Phi_u\,|\alpha\rangle\,\langle\alpha|\,\Delta\Phi_v\,|\beta\rangle\,,\end{aligned} \tag{1.35}$$

where we separated trace over the electronic and bath degrees of freedom, expressed $\hat{H}_{\rm R}$ in energy representation, and rewrote it into the transition frequencies between the reservoir energy levels $\omega_{\alpha\beta} = (E_\alpha - E_\beta)/\hbar$. The function

$$f(E_\alpha) \equiv \langle\alpha|\,\rho^{\rm eq}_{\rm R}\,|\alpha\rangle = \frac{e^{-E_\alpha/k_{\rm B}T}}{\sum_\beta e^{-E_\beta/k_{\rm B}T}} \tag{1.36}$$

is the Boltzmann function of the thermal distribution. Performing an integration over t yields

$$\tilde{C}_{uv}(\omega) = \frac{2\pi}{\hbar}\sum_{\alpha\beta} f(E_\beta)\,\langle\beta|\,\Delta\Phi_u\,|\alpha\rangle\,\langle\alpha|\,\Delta\Phi_v\,|\beta\rangle\,\delta(\omega+\omega_{\alpha\beta})\;, \tag{1.37a}$$

$$\tilde{C}_{vu}(\omega) = \frac{2\pi}{\hbar}\sum_{\alpha\beta} f(E_\alpha)\,\langle\beta|\,\Delta\Phi_u\,|\alpha\rangle\,\langle\alpha|\,\Delta\Phi_v\,|\beta\rangle\,\delta(\omega+\omega_{\beta\alpha})\;. \tag{1.37b}$$

Using the identity

$$e^{-E_\beta/k_{\rm B}T}\delta(\omega+\omega_{\alpha\beta}) = e^{-(E_\alpha+\hbar\omega)/k_{\rm B}T}\delta(\omega-\omega_{\beta\alpha}) \tag{1.38}$$

we get

$$\tilde{C}_{uv}(\omega) = e^{-\hbar\omega/k_{\rm B}T}\tilde{C}_{vu}(-\omega)\;, \tag{1.39}$$

which relates negative frequencies of correlation function to positive ones. One can also rewrite Eq. (1.39) as

$$\tilde{C}_{uv}(\omega) = \frac{\tilde{C}_{uv}^{(\pm)}(\omega)}{1 \pm e^{-\hbar\omega/k_{\mathrm{B}}T}} = (1 + n(\omega))\, \tilde{C}_{uv}^{(-)}(\omega)\ , \tag{1.40}$$

where

$$n(\omega) = \frac{1}{e^{\hbar\omega/k_{\mathrm{B}}T} - 1} \tag{1.41}$$

is the Bose-Einstein distribution function.

1.5.2 Correlation Function of a Damped Harmonic Oscillator

In the subsequent simulations, we describe the reservoir by so-called multi-mode Brownian oscillators model. The quantum correlation function of a harmonic oscillator can be exactly derived from its classical counterpart thanks to a special property – its independence on temperature. This derivation is beyond scope of this work. Ref. [11] devotes a lot of attention to this topic, namely Chapter 8, including appendixes 8B, 8D and 8E. One can find some interesting remarks also in Ref. [12].

We will use only limiting case of an overdamped harmonic oscillator, here. Its correlation function reads

$$C(t) = -i\hbar\lambda\Lambda\ e^{-\Lambda|t|}\ \operatorname{sgn} t + \lambda\Lambda\hbar \coth\left(\frac{\beta\hbar\Lambda}{2}\right)\ e^{-\Lambda|t|} + \frac{4\Lambda\lambda}{\beta} \sum_{n=1}^{\infty} \frac{\nu_n e^{-\nu_n|t|}}{{\nu_n}^2 - \Lambda^2}, \tag{1.42}$$

where

$$\nu_n \equiv \frac{2\pi n}{\hbar\beta}, \quad \beta \equiv \frac{1}{k_{\mathrm{B}}T}, \quad \Lambda \equiv \frac{1}{\tau_{\mathrm{C}}}, \tag{1.43}$$

k_{B} is Boltzmann constant, T thermodynamic temperature, τ_{C} coherence time of relaxation and λ is reorganisation energy. Frequencies ν_n are so-called Matsubara frequencies.

1.6 Markov Approximation

The Markov approximation is very useful way how to make computations based on the Quantum Master Equation more numerically feasible. The QME is an integro-differential equation, hence it represents a much more complicated problem for numerical solution than ordinary differential equations. The Markov approximation is based, as explained in Ref. [6], on an assumption that $\hat{H}_{\mathrm{S-R}}$ is much smaller than $\hat{H}_{\mathrm{S}}$. Therefore the presence of $\hat{H}_{\mathrm{S-R}}$ causes time evolution much slower than the corresponding evolution caused by the $\hat{H}_{\mathrm{S}}$. The slow evolution can be separated in the interaction representation, Eq. (1.16), which leads us to

$$\begin{aligned}\rho_{\mathrm{S}}(t-\tau) &= \hat{U}_{\mathrm{S}}(t-\tau-t_0)\rho_{\mathrm{S}}^{(\mathrm{I})}(t-\tau)\hat{U}_{\mathrm{S}}^{+}(t-\tau-t_0)\\ &\approx \hat{U}_{\mathrm{S}}(-\tau)\hat{U}_{\mathrm{S}}(t-t_0)\rho_{\mathrm{S}}^{(\mathrm{I})}(t)\hat{U}_{\mathrm{S}}^{+}(t-t_0)\hat{U}_{\mathrm{S}}^{+}(-\tau)\\ &= \hat{U}_{\mathrm{S}}(-\tau)\rho_{\mathrm{S}}(t)\hat{U}_{\mathrm{S}}^{+}(-\tau)\ .\end{aligned} \tag{1.44}$$

Applying this to the QME (1.29), we receive the final equation

$$\begin{aligned}\frac{d}{dt}\rho_{\mathrm{S}}^{(\mathrm{I})}(t) =& -\frac{i}{\hbar}\sum_u \langle\Phi_u\rangle\left[\hat{P}_u^{(\mathrm{I})}(t),\rho_{\mathrm{S}}^{(\mathrm{I})}(t)\right]_-\\ &-\sum_{uv}\int_0^t d\tau\,\Big(C_{uv}(t-\tau)\left[\hat{P}_u^{(\mathrm{I})}(t),\hat{P}_v^{(\mathrm{I})}(\tau)\rho_{\mathrm{S}}^{(\mathrm{I})}(t)\right]_-\\ &-C_{uv}(-t+\tau)\left[\hat{P}_u^{(\mathrm{I})}(t),\rho_{\mathrm{S}}^{(\mathrm{I})}(t)\hat{P}_v^{(\mathrm{I})}(\tau)\right]_-\Big)\ ,\end{aligned} \tag{1.45}$$

which is no longer integro-differential, but an ordinary differential, because $\rho(t)$ can now be taken out of the integral and the integral can be explicitly calculated as a function of t. We set $t_0 = 0$ without loss of generality (WLOG).

In numerical calculation, we use Eq. (1.45) in a form

$$\hat{\Lambda}_u(t) \equiv \sum_v \int_0^t d\tau\, C_{uv}(\tau)\hat{P}_v^{(\mathrm{I})}(-\tau)\ , \tag{1.46a}$$

$$\hat{H}_{\mathrm{S}}^{(\mathrm{eff})} \equiv \hat{H}_{\mathrm{S}} + \sum_u \hat{P}_u\left(\langle\Phi_u\rangle_{\mathrm{R}} - i\hbar\hat{\Lambda}_u(t)\right)\ , \tag{1.46b}$$

$$\frac{d}{dt}\rho(t) = -\frac{i}{\hbar}\left(\hat{H}_{\mathrm{S}}^{(\mathrm{eff})}\rho_{\mathrm{S}}(t) - \rho_{\mathrm{S}}(t)\hat{H}_{\mathrm{S}}^{(\mathrm{eff})+}\right) + \sum_u\left(\hat{P}_u\rho_{\mathrm{S}}(t)\hat{\Lambda}_u^{+}(t) - \hat{\Lambda}_u(t)\rho_{\mathrm{S}}(t)\hat{P}_u\right)\ . \tag{1.46c}$$

If the relation (1.46a) converges to a constant value on a considerably shorter time scale compared to a characteristic time evolution of the system, additional approximation can be made by using

$$\hat{\Lambda}_u^{\infty} \equiv \hat{\Lambda}_u(+\infty) \tag{1.47}$$

in Eq. (1.46c) instead of Eq. (1.46a). Such equations are called *Redfield equations*, while Eqs. (1.46) are called *Redfield equations with time-dependent Redfield tensor*.

1.7 Secular Approximation

The secular approximation is an additional approximation imposed on Eq. (1.46c), often used in publications related to non-linear optical experiments. It makes numerical solution of Eq. (1.46c) faster, simpler, and it stabilizes it significantly, as we show later. It moreover leads to the canonical thermal equilibrium even in cases when (1.46c) gives completely wrong answers.

Let us rewrite equation (1.46c) as

$$\frac{d}{dt}\rho_{\mathrm{S}ab}^{(\mathrm{exc})}(t)\bigg|_{\mathrm{diss}} = -\sum_{cd}\mathcal{R}_{ab,cd}^{(\mathrm{exc})}(t)\ \rho_{\mathrm{S}cd}^{(\mathrm{exc})}(t)\ , \tag{1.48}$$

where $\mathcal{R}(t)$ is *time-dependent Redfield tensor* and "diss" on the left equation side denotes, that we take only the dissipation part of the system density operator time derivative. The secular approximation consists of neglecting terms of $\mathcal{R}^{(\mathrm{exc})}$ which do not represent population transfer ($a = b, c = d$) nor coherence dephasing ($a \neq b, a = c, b = d$). Such terms oscillate rapidly in the interaction picture (see Ref. [6] Eq. (3.294) for more detailed information) and therefore almost do not contribute.

1.8 Thermodynamic Equilibrium

The QME (1.29) involves relaxation of the system to thermodynamic equilibrium. In various approximation of the QME, different equilibrium is obtained. As explained in Ref. [6] in detail, the secular approximation leads to the canonical thermodynamic equilibrium

$$\rho_{\mathrm{S}}^{\mathrm{eq}} = \frac{e^{-\hat{H}_{\mathrm{S}}/k_{\mathrm{B}}T}}{\mathrm{Tr}\left(e^{-\hat{H}_{\mathrm{S}}/k_{\mathrm{B}}T}\right)}\ . \tag{1.49}$$

However, if we use the Markov approximation without the secular approximation, it cannot be proven that system settles to the canonical thermal equilibrium (1.49) nor that we receive positive probabilities of occupancy of states for all times. In fact, as our numerical model shows, for certain parameters we receive negative probabilities even in thermal equilibrium, which is due to specific failure of the Markov approximation discussed in the Chapter 3.

May and Kühn in Ref. [6] also claim that the QME itself, with no additional approximations, leads to canonical thermodynamic equilibrium (1.49) as well. However, their proof is incorrect – there is a correction to Eq. (1.49) which changes basis in which the relaxation takes place from the exciton basis to another one. It happens, because the described system is not closed. (Thermodynamics demands relaxation to canonical thermal equilibrium for

closed systems only.) There are articles supporting and giving reasons for this result, e.g. the article [13]. We devote the Section 3.3 to this problem.

1.9 Fourier Transform Solution of the QME

We can rewrite the QME (1.30) into the superoperator formalism as

$$\frac{d}{dt}\rho_{\mathrm{S}}(t) = -i\mathcal{L}\rho_{\mathrm{S}}(t) - \int_{t_0}^{t} d\tau\ \mathcal{M}(t-\tau)\rho_{\mathrm{S}}(\tau)\ , \tag{1.50}$$

where $\mathcal{L}$ is Liouville superoperator (1.8) and $\mathcal{M}(t)$ is superoperator representing all terms affecting ρ_{S} under integral over τ in (1.30). Let us denote

$$\overline{\mathcal{M}}(t) = \Theta(t)\mathcal{M}(t)\ , \tag{1.51}$$

$$\bar{\rho}(t) = \Theta(t)\rho(t)\ . \tag{1.52}$$

Now we can rewrite Eq. (1.50) as

$$\frac{d}{dt}\bar{\rho}_{\mathrm{S}}(t) = -i\mathcal{L}\bar{\rho}_{\mathrm{S}}(t) - \int_{-\infty}^{\infty} d\tau\ \overline{\mathcal{M}}(t-\tau)\bar{\rho}_{\mathrm{S}}(\tau) + \rho_{\mathrm{S}}^{0}\,\delta(t)\ , \tag{1.53}$$

where δ-function represents initial condition $\bar{\rho}_{\mathrm{S}}(0) = \rho_{\mathrm{S}}^{0}$. Since $\bar{\rho}_{\mathrm{S}}(t) = 0$ and and $\overline{\mathcal{M}}(t) = 0$ for $t < 0$, they form natural boundary for the integral on rhs of Eq. (1.50) and it is replaced by convolution. (If we WLOG define $t_0 = 0$, in addition.)

We take Fourier transform of (1.53)

$$i\omega\tilde{\bar{\rho}}_{\mathrm{S}}(\omega) = -i\mathcal{L}\tilde{\bar{\rho}}_{\mathrm{S}}(\omega) - \tilde{\overline{\mathcal{M}}}(\omega)\tilde{\bar{\rho}}_{\mathrm{S}}(\omega) + \rho_{\mathrm{S}}^{0}\ \ , \tag{1.54}$$

which gives us the solution

$$\tilde{\bar{\rho}}_{\mathrm{S}}(\omega) = \frac{1}{i\omega + i\mathcal{L} + \tilde{\overline{\mathcal{M}}}(\omega) + \varepsilon}\,\rho_{\mathrm{S}}^{0} \equiv \mathcal{G}_{\varepsilon}(\omega)\rho_{\mathrm{S}}^{0} \tag{1.55}$$

in frequency domain. $\mathcal{G}_{\varepsilon}(\omega)$ is Green's function and ε is small positive value which represents regularization in which $\rho_{\mathrm{S}}(t) = 0$ for $t < 0$. By performing inverse Fourier Transform we have

$$\bar{\rho}_{\mathrm{S}}(t) = \lim_{\varepsilon\to 0+}\frac{1}{2\pi}\int_{-\infty}^{\infty} d\omega\ e^{i\omega t}\,\mathcal{G}_{\varepsilon}(\omega)\rho_{\mathrm{S}}^{0}\ . \tag{1.56}$$

1.9.1 Discrete Fourier Transform

An analytic solution of QME using Fourier transform is out of question. We therefore rewrite all the above expressions into the discrete Fourier transform (DFT), which can be directly used for numerical solution of QME.

In the DFT we cover interval $t \in \left[-\frac{1}{2}T_{max}, \frac{1}{2}T_{max}\right]$ by N points in which we know function values of used functions. We can in addition define

$$\Delta t \equiv \frac{T_{max}}{N} \,, \tag{1.57}$$

$$\Omega_{max} = \frac{2\pi N}{T_{max}} \,. \tag{1.58}$$

In this normalisation, the DFT has a form

$$\tilde{f}(\omega_s) = \sum_{r=1}^{N} f(t_r) e^{-2\pi i (r-1)(s-1)/N} \,, \tag{1.59a}$$

$$f(t_r) = \frac{1}{N} \sum_{s=1}^{N} \tilde{f}(\omega_s) e^{2\pi i (r-1)(s-1)/N} \,, \tag{1.59b}$$

which has same properties when acting on convolution and function derivative as Fourier transform in normalisation used above, namely

$$\widetilde{f'(t)}[\omega] = i\omega \tilde{f}(\omega) \,, \tag{1.60a}$$

$$\widetilde{f(t) * g(t)}[\omega] = \tilde{f}(\omega)\tilde{g}(\omega) \,, \tag{1.60b}$$

where discrete convolution is defined as

$$f(t) * g(t)[t_n] \equiv \sum_{m=-\infty}^{\infty} f(t_n) g(t_{m-n}) \,. \tag{1.61}$$

Now we rewrite Eq. (1.53) in discretised form

$$\frac{d}{dt}\rho_{\mathrm{S}}(t_r) = -i\mathcal{L}\rho_{\mathrm{S}}(t_r) - \sum_{m=-\infty}^{\infty} \mathcal{M}(t_r - t_m)\rho_{\mathrm{S}}(t_m)\Delta t + \rho_{\mathrm{S}}^0 \frac{1}{\Delta t}\,\delta_{1r} \,. \tag{1.62}$$

One Δt clearly emerges from discretisation of convolution integral in Eq. (1.53) while the other one fixes normalisation of discretised δ-function – if it is equal to $\frac{1}{\Delta t}$ for $r = 1$, which is interval of length Δt, its integral over t is the same as of the original δ-function.

To perform numerics, we use Mathematica®, which internally uses FFT algorithm [14, 15], for the DFT.

1.9.2 Numerical Handling of the Regularization

As we can see from Eq. (1.55), Inverse Fourier transform is dependent on a small imaginary part of ω represented by ε-regularization. We would like to write the limit (1.56) $\varepsilon \to 0$ in terms of the DFT which would allow us to obtain solution $\rho_{\mathrm{S}}(t)$ non-zero only for $t > 0$. Value of ε has to be sufficiently small so that the result wouldn't depend on it, but at the same time it has to be big enough compared to discretisation of time axis, $\varepsilon \approx \Delta t$. (If it were not, the DFT wouldn't even notice there is any ε!) So now we have a problem since clearly our result depends on ratio of ε and Δt.

Luckily there is a way out of the trouble. This ε-sensitivity is characteristic only for functions which do not tend to zero for $|t| \to \infty$ but to finite constant. (Solution of QME doesn't tend to zero since populations end in constant thermal equilibrium.)

Let $w(t)$ be typical diagonal element of $\rho_{\mathrm{S}}(t)$, solution of QME. Let

$$\lim_{t\to\infty} w(t) = w_0 \neq 0, \tag{1.63}$$

$$w(t) = w(t)\Theta(t), \tag{1.64}$$

hold. We introduce

$$w^{\blacktriangle}(t) = e^{-\alpha t} w(t)\ , \tag{1.65a}$$

$$w^{\blacktriangledown}(t) = e^{\alpha t} w(t)\ , \tag{1.65b}$$

where $\alpha > 0$ is additional parameter. Because $w^{\blacktriangle}(t)$, unlike $w(t)$, is L^2-integrable, its Fourier transform $\widetilde{w^{\blacktriangle}}(\omega)$ is L^2-integrable and therefore it does not have poles on real axis (and doesn't need ε-regularization).

Parameter α has a very similar meaning as ε, which we can see from

$$\widetilde{(w'(t))^{\blacktriangle}} = (i\omega + \alpha)\, \widetilde{w^{\blacktriangle}}(\omega)\ , \tag{1.66}$$

where α stands for small imaginary part of ω, like ε. However it is not so localised in $\omega = 0$. Its value has to be determined from numerical behaviour of the DFT. It turns out that for α too small ultra-fast oscillations appear in frequency domain after applying the DFT, while for α too big regularization doesn't fulfil its purpose. We use the value $\alpha \approx T_{max}/7$.

1.9.3 Convergence of the DFT

While for solving differential equations, the methods used here are very precise and converge is fast, the convergence of the DFT is a bit more problematic. Namely the thermal equilibrium to which the system converges for $t \to \infty$ is a "local" effect in the differential equation (and therefore the difference between the numerical and the real solution of the equation is minimal), in the DFT method it is a "global" effect (we need all frequencies for its description) and its error can be much bigger. For this reason, a question of the convergence is crucial.

To investigate the DFT convergence, we need to know the long time limit solution of the QME. If we take the QME in the form (1.50) and we demand the solution to be constant, then we can conclude that the limiting solution of the QME has to be an eigenvector of the superoperator

$$\mathcal{Y}^{\infty}_{\mathrm{QME}} \equiv -i\mathcal{L} + \int_0^{\infty} d\tau\, \mathcal{M}(\tau) \tag{1.67}$$

corresponding to the eigenvalue 0. One can obtain this eigenvector by numerical integration of superoperator (1.67)

Fig. 1.1 shows the dependence of the maximum[1] relative difference

$$\frac{\Delta\rho}{\mathrm{Tr}\,\rho} \equiv \max_{ij} \left| \frac{\left(\rho^{\#}_{\infty} - \rho^{\mathrm{eig}}_{\infty}\right)_{ij}}{\mathrm{Tr}\,\rho^{\mathrm{eig}}_{\infty}} \right| \tag{1.68}$$

between limiting numerical solutions of the QME, $\rho^{\#}_{\infty}$, calculated by the DFT with # steps and the eigenvector of the superoperator (1.67), $\rho^{\mathrm{eig}}_{\infty}$, respective to eigenvalue 0.

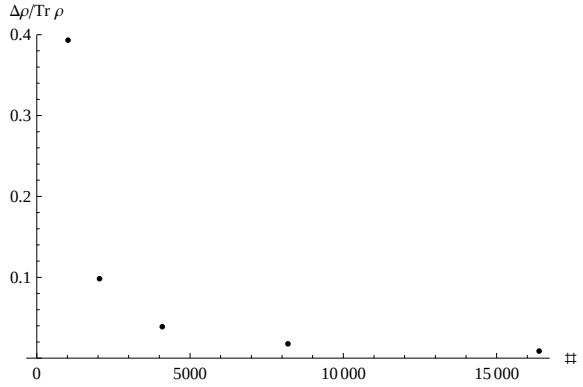

Figure 1.1: Relative error of the DFT dependent on number of steps.

For # = 8192 is the error of the DFT sufficiently small. It is the value we use for all calculations performed in this work.

[1]The maximum is taken over all matrix elements ij.

1.10 Initial Conditions Created by an Ultra-Short Laser Pulse

If we want to use QME and Redfield equations equations for description of time evolution of real system, we need to know how does an excitation by laser pulse look like and use it to set the initial condition.

Let us assume a relaxation-free Liouville equation, with a semi-classical light-matter interaction Hamiltonian in dipole approximation

$$\begin{aligned}\frac{d\rho_{\mathrm{S}}}{dt} &= -i\mathcal{L}\rho_{\mathrm{S}} - \frac{i}{\hbar}\left[-\hat{\mu}E(t), \rho_{\mathrm{S}}\right]_- \\ &\equiv -i\mathcal{L}\rho_{\mathrm{S}} + i\mathcal{D}(t)\rho_{\mathrm{S}}\ E(t)\ .\end{aligned} \tag{1.69}$$

We take dipole moment operator and electric field to be scalars in our simple model. The operator $\hat{\mu}$ is dipole moment operator and

$$\mathcal{D}(t)\bullet \equiv \frac{1}{\hbar}\left[\hat{\mu}E(t), \bullet\right]_- \tag{1.70}$$

is dipole moment superoperator.

We rewrite the above equation into interaction picture

$$\frac{d\rho_{\mathrm{S}}^{(\mathrm{I})}}{dt}(t) = i\mathcal{D}^{(\mathrm{I})}(t)\ \rho_{\mathrm{S}}^{(\mathrm{I})}(t)\ E(t) \tag{1.71}$$

and write its formal solution as

$$\rho_{\mathrm{S}}^{(\mathrm{I})}(t) = \rho_{\mathrm{S}}^{(\mathrm{I})}(t_0) + i\int_{t_0}^{t} \mathcal{D}^{(\mathrm{I})}(\tau)\rho_{\mathrm{S}}^{(\mathrm{I})}(\tau)\ E(\tau)\ . \tag{1.72}$$

For $t_0 < 0$, for

$$\rho_{\mathrm{S}}^{(\mathrm{I})}(t_0) = |g\rangle\langle g| \tag{1.73}$$

and for ultra-short pulse

$$E(t) = \delta(t)E_0\ , \tag{1.74}$$

Eq. (1.72) can be written as

$$\rho_{\mathrm{S}}^{(\mathrm{I})}(t) = |g\rangle\langle g| + i\mathcal{D}^{(\mathrm{I})}(0)\,|g\rangle\langle g|\ E_0\,\Theta(t)\ . \tag{1.75}$$

Finally, by substituting Eqs. (1.74) and (1.75) into Eq. (1.71) we get

$$\begin{aligned}\frac{d\rho_{\mathrm{S}}^{(\mathrm{I})}}{dt}(t) &= i\mathcal{D}^{(\mathrm{I})}(0)\left(|g\rangle\langle g| + i\mathcal{D}^{(\mathrm{I})}(0)\,|g\rangle\langle g|\ E_0\,\Theta(t)\right)\delta(t)\ E_0 \\ &= \left[iE_0\,\mathcal{D}^{(\mathrm{I})}(0)\,|g\rangle\langle g| - \frac{{E_0}^2}{2}\,\mathcal{D}^{2(\mathrm{I})}(0)\,|g\rangle\langle g|\right]\delta(t)\ .\end{aligned} \tag{1.76}$$

Here we used the identity

$$\Theta(t)\delta(t) = \frac{1}{2}\delta(t) \ . \tag{1.77}$$

(The δ-function is intrinsically symmetric.) We rewrite Eq. (1.76) to the Schrödinger picture, yielding

$$\frac{d\rho_{\mathrm{S}}}{dt}(t) = -i\mathcal{L}\rho_{\mathrm{S}}(t) + \left[iE_0\,\mathcal{U}^{+}(-t_0)\mathcal{D}\,|g\rangle\langle g| - \frac{{E_0}^2}{2}\,\left(\mathcal{U}^{+}(-t_0)\mathcal{D}\right)^2|g\rangle\langle g|\right]\delta(t) \ . \tag{1.78}$$

This result can be interpreted so that the ultra-short laser pulse sets the initial condition to be used with the equation of motion to

$$\rho_{\mathrm{S}}^{0} = |g\rangle\langle g| + iE_0\,\mathcal{U}^{+}(-t_0)\mathcal{D}\,|g\rangle\langle g| - \frac{{E_0}^2}{2}\,\left(\mathcal{U}^{+}(-t_0)\mathcal{D}\right)^2|g\rangle\langle g| \ . \tag{1.79}$$

It should be noted that $\mathcal{U}^{+}(-t_0)$ is just a phase factor and since $|g\rangle\langle g|$, $\mathcal{D}\,|g\rangle\langle g|$ and $\mathcal{D}^2\,|g\rangle\langle g|$ belong to different blocks of ρ_{S}, whose evolutions are independent for the model Hamiltonian used in the chapters that follow, it can be WLOG chosen as

$$\mathcal{U}^{+}(-t_0) = \mathbb{1} \ . \tag{1.80}$$

Chapter 2

System Model

2.1 Hamiltonian

The following system Hamiltonian construction is based on the article [16].

2.1.1 Monomer Hamiltonian

Let us recall Hamiltonian (1.14) and specify its particular form for a studied system. First we consider molecule which can be in an electronic ground state or an electronic excited state with energies ε_g, ε_e, respectively. Besides electron excitation energies, it has some vibrational degrees of freedom (DOF) connected with the movement of the nuclei. They generally depend on many coordinates, but we will replace them by generalized coordinate Q in our model. We can write the Hamiltonian in the form

$$\hat{H}^{\mathrm{m}} = (\varepsilon_g + V_g(Q)) \left|g\right\rangle \left\langle g\right| + (\varepsilon_e + V_e(Q)) \left|e\right\rangle \left\langle e\right| \ . \tag{2.1}$$

Now we rearrange the terms in Eq. (2.1) and separate the system, the reservoir and the interaction part

$$\begin{aligned} \hat{H}^{\mathrm{m}} &= \varepsilon_g \left|g\right\rangle \left\langle g\right| + \varepsilon_e \left|e\right\rangle \left\langle e\right| + V_g(Q) \left(\left|g\right\rangle \left\langle g\right| + \left|e\right\rangle \left\langle e\right|\right) + (V_e(Q) - V_g(Q)) \left|e\right\rangle \left\langle e\right| \\ &= \varepsilon_g \left|g\right\rangle \left\langle g\right| + \varepsilon_e \left|e\right\rangle \left\langle e\right| + V_g(Q) \, \mathbb{1} + \Phi(Q) \left|e\right\rangle \left\langle e\right| \\ &= \hat{H}'^{\mathrm{m}}_{\mathrm{S}} + \hat{H}'^{\mathrm{m}}_{\mathrm{R}} + \hat{H}'^{\mathrm{m}}_{\mathrm{S-R}} \ . \end{aligned} \tag{2.2}$$

Here

$$\hat{H}'^{\mathrm{m}}_{\mathrm{S}} \equiv \varepsilon_g \left|g\right\rangle \left\langle g\right| + \varepsilon_e \left|e\right\rangle \left\langle e\right| \ , \tag{2.3a}$$

$$\hat{H}'^{\mathrm{m}}_{\mathrm{R}} \equiv V_g(Q) \, \mathbb{1} \ , \tag{2.3b}$$

$$\hat{H}'^{\mathrm{m}}_{\mathrm{S-R}} \equiv \Phi(Q) \left|e\right\rangle \left\langle e\right| \ , \tag{2.3c}$$

Symbol $\mathbb{1}$ represents an unit operator on the electronic Hilbert space, and the operators $V_g(Q)$, $V_e(Q)$ represent energies of all nuclear DOF depending on generalized coordinate

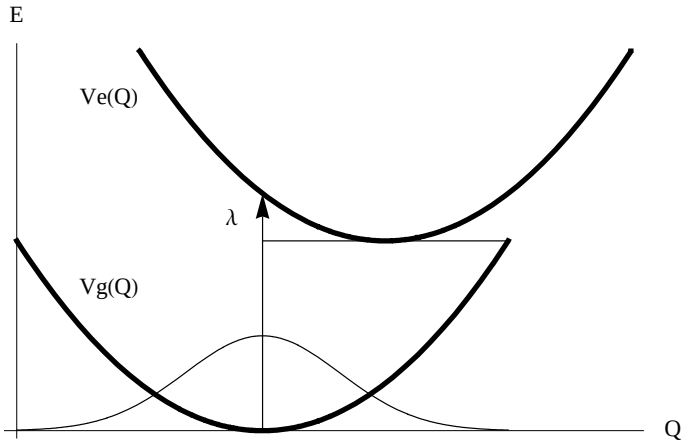

Figure 2.1: Excitation between shifted harmonic potentials.

Q in ground and excited electronic state, respectively. In our model, we consider $V_g(Q)$, $V_e(Q)$ to be mutually shifted harmonic potentials. (See the illustrating Fig. 2.1.) Now we write their difference as

$$\Phi(Q) \equiv V_e(Q) - V_g(Q) \;, \tag{2.4}$$

which is identical with Φ_i used in (1.22).

Only by shifting of ε_e in (2.3a) we can write $\Delta\Phi$, defined as (1.27), instead of Φ in (2.3c). Therefore

$$\hat{H}^{\mathrm{m}}_{\mathrm{S}} = \epsilon_g \left|g\right\rangle \left\langle g\right| + \epsilon_e \left|e\right\rangle \left\langle e\right| \;, \tag{2.5a}$$

$$\hat{H}^{\mathrm{m}}_{\mathrm{R}} = V_g(Q)\; \mathbb{1} \;, \tag{2.5b}$$

$$\hat{H}^{\mathrm{m}}_{\mathrm{S-R}} = \Delta\Phi(Q) \left|e\right\rangle \left\langle e\right| \;, \tag{2.5c}$$

and

$$\epsilon_g \equiv \varepsilon_g \;, \tag{2.6a}$$

$$\epsilon_e \equiv \varepsilon_e + \left\langle \Phi(Q) \right\rangle_{\mathrm{R}} \;. \tag{2.6b}$$

$\Delta\Phi(Q)$ is described through correlation functions by its mean value. If Q_{g_0} denotes the value of the coordinate Q in the minimum of $V_g(Q)$ and analogously for Q_{e_0}, then the difference

$$\lambda = V_e(Q_{g0}) - V_e(Q_{e0}) \;, \tag{2.7}$$

is called reorganisation energy. It is one of the parameters of the correlation function (1.42). (See Fig. 2.1.)

As we can see from structure of Quantum Master Equation, $\hat{H}^{\mathrm{m}}_{\mathrm{R}}$ does not act on the system density operator. The reservoir acts on the system through $\hat{H}^{\mathrm{m}}_{\mathrm{S-R}}$ which can be expressed by the means of correlation functions (1.26) in second order perturbation theory.

2.1.2 Aggregate Hamiltonian

The system we further examine in this work, is an aggregate of n molecules, where each of them is supposed to be in its ground state $|g\rangle$ or in first excited state $|e\rangle$. Let us now concentrate on constructing its Hamiltonian.

We assume that only states where one or two molecules of the aggregate are excited have an effect on calculating of an optical spectra. We denote them as

$$|i\rangle \equiv |g_1\rangle \dots |g_{i-1}\rangle |e_i\rangle |g_{i+1}\rangle \dots |g_n\rangle \ , \tag{2.8a}$$

$$|i<j\rangle \equiv |g_1\rangle \dots |g_{i-1}\rangle |e_i\rangle |g_{\dots}\rangle |e_j\rangle |g_{j+1}\rangle \dots |g_n\rangle \ , \tag{2.8b}$$

and refer to them as to one and two-exciton states, respectively. We also use the notation

$$|I\rangle = \begin{cases} |i\rangle & \text{for } I = i \leq n \\ \\ |i<j\rangle & \text{for } I > n,\ i(I) < j(I) \end{cases} \tag{2.9}$$

if it is necessary to work with whole basis of one and two-exciton states together.

The Hamiltonian of the aggregate is

$$\begin{aligned} \hat{H}_{\mathrm{S}} = &\sum_u \epsilon_u |u\rangle\langle u| + \sum_{u\neq v} \left(J_{uv} |u\rangle\langle v| + \mathrm{c.c}\right) + \sum_{u<v} \left(\epsilon_u + \epsilon_v\right) |u<v\rangle\langle u<v| \\ &+ \sum_{\substack{u<v,\, r<s \\ \neg(u=r\wedge v=s)}} \left(j_{rsuv} |u<v\rangle\langle r<s| + \mathrm{c.c}\right) \ , \end{aligned} \tag{2.10}$$

where ϵ_i represents electronic excitation energy of i-th molecule, while J_{uv}, j_{rsuv} represent mutual interaction energies of the particular molecules. We can rewrite the Hamiltonian, Eq. (2.11), into the form

$$\begin{aligned} \hat{H}_{\mathrm{S}} = &\sum_u \left(\Delta\epsilon_u + \Omega\right) |u\rangle\langle u| + \sum_{u\neq v} \left(J_{uv} |u\rangle\langle v| + \mathrm{c.c}\right) \\ &+ \sum_{u<v} \left(\Delta\epsilon_u + \Delta\epsilon_v + 2\Omega\right) |u<v\rangle\langle u<v| \\ &+ \sum_{\substack{u<v,\, r<s \\ \neg(u=r\wedge v=s)}} \left(j_{rsuv} |u<v\rangle\langle r<s| + \mathrm{c.c}\right) \ , \end{aligned} \tag{2.11}$$

where

$$\Delta\epsilon_i \equiv \epsilon_i - \Omega \ , \tag{2.12}$$

represents differences between electronic energies of i-th molecule and Ω is the energy of the optical excitation, typically much larger that differences of energies of molecules. When performing calculations inside one- or two-exciton density matrix block, Ω can be omitted, because it represents only a constant shift of the energy. However, one cannot do this when examining the coherences between these blocks.

2.2 Correlation Functions

In our model, we always assume interaction with harmonic potential described by correlation functions (1.42). Probably the simplest model is to assume that fluctuations on each molecule are local and therefore independent of other molecules. In this case it holds

$$C_{ij}(t) = \frac{1}{\hbar^2}\delta_{ij}C_i(t) \tag{2.13}$$

for 1-exciton states in local basis.

Correlation functions for 2-exciton states can be constructed unambiguously from this assumption. Beginning with definition (1.26) we write

$$\begin{aligned} C_{i<j,u<v}(t) &= \langle (\Delta\Phi_i(t) + \Delta\Phi_j(t))\,(\Delta\Phi_u(0) + \Delta\Phi_v(0)) \rangle_{\mathrm{R}} \\ &= (\delta_{iu} + \delta_{iv})\,C_i(t) + (\delta_{ju} + \delta_{jv})\,C_j(t)\ , \end{aligned} \tag{2.14}$$

which means not only that the diagonal elements of $C_{i<j,u<v}$ are nonzero, but also that those, for which one excited molecule in states $|i<j\rangle$, $|u<v\rangle$ is shared, are nonzero.

We can also consider a model in which fluctuations on molecules are not strictly local, but there are cross-correlation terms exponentially decaying with molecular distance. In this case the correlation functions are not restricted by Eq. (2.13) and their reorganisation energy is given as

$$\lambda_{ij} = \lambda_0 e^{-\alpha f(i,j)}\ , \tag{2.15}$$

where

$$f(i,j) = f(j,i) \tag{2.16a}$$
$$f(i,i) = 0 \tag{2.16b}$$

is distance function of molecules, for example

$$f(i,j) = |i-j| \tag{2.17}$$

for an acyclic aggregate or

$$f(i,j) = \min_{k\in\mathbb{Z}} |i-j-kn| \tag{2.18}$$

for a cyclic aggregate. Correlation functions for 2-exciton states are then given by

$$C_{i<j,u<v}(t) = C_{iu}(t) + C_{iv}(t) + C_{ju}(t) + C_{jv}(t)\ , \tag{2.19}$$

2.3 Asymptotic Behaviour of a Markov Approximation-Based Algorithm

Let n be number of the molecules in considered aggregate and N is the length of basis of the used Hilbert space. Then the density matrix, whose evolution we calculate, has N^2 elements. Considering only 1-exciton and 2-exciton states,

$$N = n + \frac{n(n-1)}{2} = \mathrm{O}\left(n^2\right) \ . \tag{2.20}$$

In Eq. (1.45), which we numerically solve, integrals of correlation function (1.46a) have to be calculated. There is N of them and each has N^2 elements, so we need N^3 time-dependent functions to be calculated. Components of the evolution superoperator, relevant for the 2D-spectra calculations mentioned in the Introduction, give amplitudes of the transition, among the elements of the 1-exciton density matrix block and the 1-exciton block, and coherences between the 1-exciton and 2-exciton density matrix blocks. Therefore there is $(2nN)^2$ elements of evolution superoperator to be calculated.

Hence asymptotic memory and time evaluation requirements of the algorithm are $\mathrm{O}(n^6)$.

2.4 Direct Solution of the QME by Expanding Correlation Functions into Exponential Functions

Taking closer look on equation (1.29), we can see that if the correlation function $C_{uv}(t)$ has property

$$C_{uv}(t+\tau) = C_{uv}(t)C_{uv}(\tau) \ , \tag{2.21}$$

(being linear or exponential function), or if it is sum of such terms

$$C_{uv}(t+\tau) = \sum_{\mu} C^{\mu}_{uv}(t)C^{\mu}_{uv}(\tau) \ , \tag{2.22}$$

we can take it outside the integral in rhs of QME and rewrite it into an ordinary differential equation

$$\begin{aligned}\frac{d}{dt}\rho^{(\mathrm{I})}_{\mathrm{S}}(t) = &-\frac{i}{\hbar}\sum_{u}\langle\Phi_u\rangle\left[\hat{P}^{(\mathrm{I})}_{u}(t), \rho^{(\mathrm{I})}_{\mathrm{S}}(t)\right]_{-} \\ &-\sum_{uv\mu}\left[\hat{P}^{(\mathrm{I})}_{u}(t), C^{\mu}_{uv}(t)\int\limits_{t_0=0}^{t} d\tau\, C^{\mu}_{uv}(-\tau)\hat{P}^{(\mathrm{I})}_{v}(\tau)\rho^{(\mathrm{I})}_{\mathrm{S}}(\tau) - h.c.\right]_{-} \ ,\end{aligned} \tag{2.23}$$

where the transposition in Hermitian conjugation is related to "inner" indices on Hilbert space on which all used operators are defined, not to indices u, v. We can rewrite this

equation to the form more convenient for numerical calculation

$$\frac{d}{dt}\rho_{\mathrm{S}}^{(\mathrm{I})}(t) = -\frac{i}{\hbar}\sum_{u}\langle\Phi_u\rangle\left[\hat{P}_u^{(\mathrm{I})}(t),\rho_{\mathrm{S}}^{(\mathrm{I})}(t)\right]_- - \sum_{uv\mu}\left[\hat{P}_u^{(\mathrm{I})}(t), C_{uv}^{\mu}(t)\gamma_{uv}^{\mu}D_v^{\mu}(t) - C_{uv}^{\mu\,*}(t)\gamma_{uv}^{\mu\,*}D_v^{\mu+}(t)\right]_- , \tag{2.24a}$$

$$\frac{d}{dt}\hat{D}_v^{\mu}(t) = e^{\omega_\mu t}\hat{P}_v^{(\mathrm{I})}(t)\rho_{\mathrm{S}}^{(\mathrm{I})}(t) , \tag{2.24b}$$

providing

$$C_{uv}^{\mu}(t) = \gamma_{uv}^{\mu}e^{-\omega_\mu t} , \tag{2.25}$$

where γ_{uv}^{μ} are time independent. This reduces the size of $\hat{D}$-matrices by one index saving memory during calculation.[1] Properties (2.22), (2.25) are indeed satisfied in case of the correlation function (1.42) if we do not take the Matsubara sum to infinity, but only to some finite number. In this case ω_μ are the Matsubara frequencies.

Similar approach of the direct QME solution by taking advantage of the particular form of correlation functions is described e.g. in the article of Tannor and Meier [17].

[1] There is furthermore a suitable numerical trick – to substitute $\hat{D}_v^{\mu}(t) = e^{-\omega_\mu t}\hat{D}_v^{\circ\mu}(t)$ preventing it from exponential growth, but we will not make this in detail, since, as shown later, this method suffers from numerical instability and cannot be used easily.

Chapter 3

Results of Numerical Computation

3.1 Failure of the Markov Approximation with Non-Secular Terms

From the numerical calculations we can see that the Markov approximation without neglecting the non-secular terms gives different thermal equilibrium than the secular approximation, Eq. (1.49). This difference is particularly sensitive to the ratio $J/\Delta\epsilon$, where J is of the same order of magnitude as interaction energies in aggregate Hamiltonian (2.10) and $\Delta\epsilon$ is in the order of magnitude of the differences between the excitation energies in the one- and two-exciton bands. For small $J/\Delta\epsilon$, the difference in detail balance is so high that negative probabilities occur.

This behaviour is a specific failure of the Markov approximation with non-secular terms. The secular approximation, which leads to the canonical thermal equilibrium, is based on an assumption that the coherence transfer terms in Eq. (1.46c) do not contribute due to their fast oscillations in the excitonic basis. Their contribution however, is not small.

Let us write Eqs. (1.46) in the superoperator form

$$\frac{d}{dt}\rho_{\mathrm{S}}(t) = \mathcal{Y}(t)\rho_{\mathrm{S}}(t) \ , \tag{3.1}$$

where $\mathcal{Y}(t)$ is the superoperator representing the action of the rhs of the Eq. (1.46c) on the density operator[1]. As the $\mathcal{Y}(t)$ becomes constant due to the correlation functions tending to zero, and $\hat{\Lambda}_u(t)$ approaches $\hat{\Lambda}_u^{\infty}$, Eq. (3.1) becomes a linear differential equation with constant coefficients

$$\frac{d}{dt}\rho_{\mathrm{S}}(t) = \mathcal{Y}^{\infty}\rho_{\mathrm{S}}(t) \ . \tag{3.2}$$

However, $\mathcal{Y}^{\infty}$ can still contain relatively big terms representing a coherence-coherence transfer.

[1] Technically, it is the sum of the time-dependent Redfield tensor $\mathcal{R}(t)$ and the effective Liouvillian $\mathcal{L}^{(\mathrm{eff})}$ defined by Eq. (1.4), with use of the effective Hamiltonian $\hat{H}_{\mathrm{S}}^{(\mathrm{eff})}$ from the Eq. (1.46b).

Eq. (3.2) has the solution

$$\rho_{\mathrm{S}}(\infty) = \lim_{t\to\infty} \exp(t\,\mathcal{Y}^{\infty})\,\rho_{\mathrm{S}}^{0} \tag{3.3}$$

for $t \to \infty$. The density matrix $\rho_{\mathrm{S}}(\infty)$ is well-defined if $\mathcal{Y}^{\infty}$ has non-positive eigenvalues. Typically there are zero eigenvalues for the vector subspace of populations and negative eigenvalues for the dying coherences. In fact, our numerical model shows that there can be even positive eigenvalues for coherences due to the coherence-coherence transfer terms. In that case, equation (3.3) diverges. Now we can see that for $t \to \infty$, $\rho_{\mathrm{S}}(t)$ cannot oscillate in the Schrödinger picture and therefore has to oscillate in the interaction picture. In that case, the Markov approximation is no longer fulfilled and it can lead to an unphysical or incorrect result.

We can conclude that the secular approximation saves the numerical stability of the model. It gives the canonical thermal equilibrium and ensures that the eigenvalues of $\mathcal{Y}^{\infty}$ are non-positive. However it cannot, from the principle, describe the coherence transfer effects, which, as we show later in this work, cannot be generally neglected and play an important role in the description of the long-lasting oscillations.

3.1.1 Markov Approximation Failure in Case of a Dimer

Let us examine the failure of the Markov approximation on a particular physical system – a dimer. We are interested in a time evolution of the one excitonic block of the density matrix and we therefore choose respective part of the Hamiltonian (2.10) as

$$\hat{H}_{\mathrm{S}} = \begin{pmatrix} \epsilon_1 & J \\ J & \epsilon_2 \end{pmatrix} . \tag{3.4}$$

Let

$$\epsilon_1 = 0 , \tag{3.5a}$$
$$\epsilon_2 = \Delta\epsilon , \tag{3.5b}$$

where $\Delta\epsilon$ is difference between the electronic excitation levels. Unlike in other numerical experiments presented in this work, we set an initial condition to be

$$\left(\rho_{\mathrm{S}}^{0}\right)_{ij} = \delta_{ij} \tag{3.6}$$

in local basis. (One of molecules is in an excited state, others are in the ground state.)

Fig. 3.1 shows the result in the excitonic basis. The Redfield equations with the Markov approximation and with the additional secular approximation are compared. In the first row, populations are plotted. At the beginning, both cases give approximately the same result, but at some critical time, equations with and without the secular approximation start to differ from each other and on the time scale much larger that coherence time τ_{C}^{i}, positivity of the Markov solution breaks down. We obtain a strongly unphysical result. In

the next row, real and imaginary part of (single) coherence is plotted in the Schrödinger picture. In the secular approximation, coherence disappears on the scale of τ_{C}^{i}. In Redfield equations, coherence prevails and it slowly stops oscillating.

We can illustrate our explanation of the Markov approximation failure on the plot of the dimer coherence in the interaction picture (Fig. 3.1) – as one can see here, until approximately τ_{C}^{i}, coherence does not oscillate. As the Markov approximation demands, it is more or less slow envelope with no fast oscillations[2]. However as the coherence stops oscillating in the Schrödinger picture (as the evolution superoperator from Eq. (3.3) becomes constant), it starts to oscillate in the interaction picture. This causes the Markov approximation failure and the populations becomes strongly negative and unphysical.

3.2 Numerical Instability in Direct Solution of the QME

We implemented the method described in the Section 2.4 in Mathematica® 6.0 and we used multiple numerical methods to solve set of differential equations (2.24) for a dimer. However we encountered severe numerical instability causing diverging ultra-fast oscillations. We therefore used the method based on convolution described in the Section 1.9 instead.

3.3 Discussion of Canonical Equilibrium in the QME

If we take the QME in the form (1.50) and want to study its constant solution and its uniqueness, we simply look for eigenvectors of the superoperator (1.67) corresponding to the eigenvalue 0. This eigenvalue was non-degenerate in cases we tested, which means the QME has unique long-time limit solution here. Moreover, our numerical results suggests that, the solution of the QME doesn't always lead to canonical equilibrium (1.49) – there are some coherences which remain non-zero even for $t \to \infty$.

This result contradicts the proof in book of May-Kühn [6], where authors claim that limit solution of the QME is canonical equilibrium. Their argumentation proofs that if there is constant solution of the QME ρ^{0}_{QME}, which has zero coherences, then its populations are distributed according to canonical equilibrium. They however do not verify that this solution satisfies the QME in its coherences part, which it doesn't. In fact, non-canonical equilibrium as unique constant solution of the QME does not contradict thermodynamics either, because the canonical equilibrium is proven to establish only in closed, canonical systems, while the QME describes an open system in interaction with reservoir.

Some articles support this result, e.g. [13]. It gives multiple reasons why equilibrium of an open system differs from the canonical one. In general, we can say that terms of the

[2]The left Fig. 3.1c shows that there are some fast oscillations of the slow envelope even in the beginning of the time evolution – this might mean that the Markov approximation prediction that oscillations of population states (Fig. 3.1a, left) are bigger than those predicted by the secular approximation (Fig. 3.1a, right), might be also wrong.

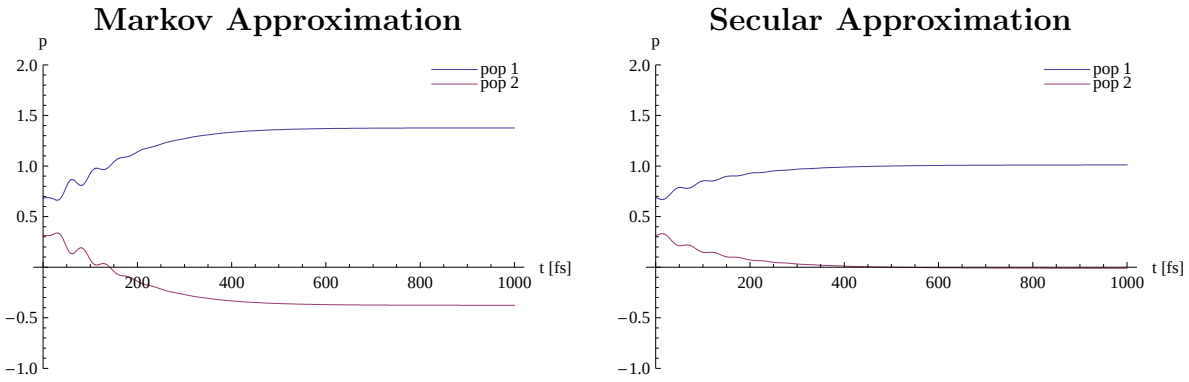

(a) Dimer populations.

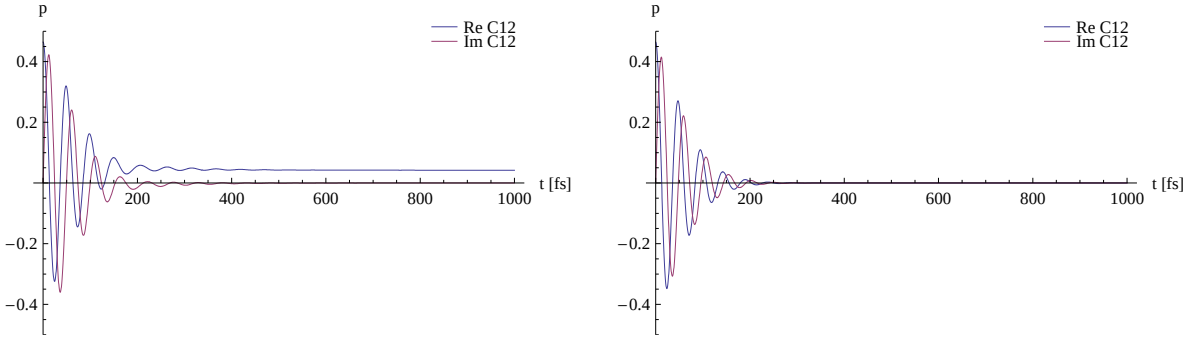

(b) Coherence 12 in the Schrödinger picture.

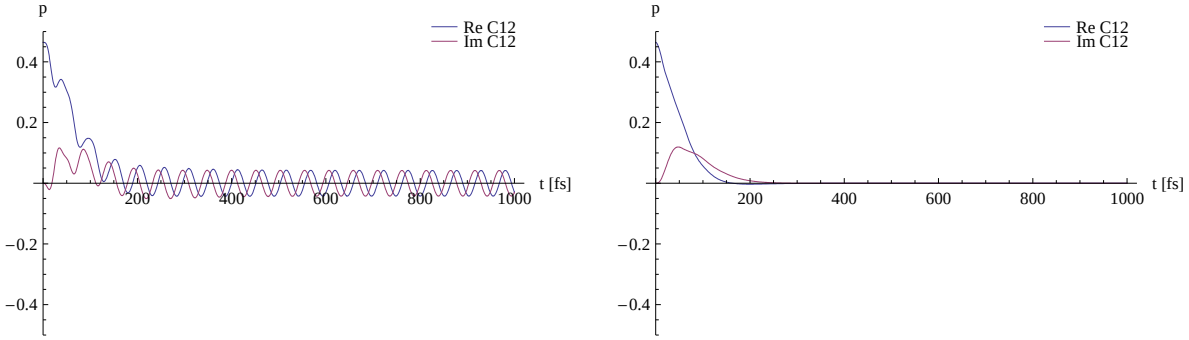

(c) Coherence 12 in the interaction picture.

Figure 3.1: Markov approximation failure.
$\Delta\epsilon = 240\ \mathrm{cm}^{-1}, J = 300\ \mathrm{cm}^{-1}, \tau_{\mathrm{C}}^{i} = 75\ \mathrm{fs}, \lambda_i = 200\ \mathrm{cm}^{-1}, T = 100\ \mathrm{K}$.

total Hamiltonian connecting system and reservoir are responsible, because they cause that (canonical) equilibrium state of the total system cannot be decomposed into system and reservoir part and the system relaxes to an equilibrium which is a superposition between them. This effectively changes the basis in which the subsystem relaxes to equilibrium.

3.4 Time Evolution of a Trimer

3.4.1 Parameters of the Numerical Experiment

In this section, we examine an aggregate of three molecules in detail. It is the simplest system, where more than one coherence is present in the one-exciton block. It is therefore not too complicated to be clearly described[3] and, on the other hand, it involves all of the coherence transfer effects we are interested in.

Let us start with the Hamiltonian

$$\hat{H}_{\mathrm{S}} = \big(0\big) \oplus \begin{pmatrix} \Delta\epsilon_1 + \Omega & J_{12} & J_{13} \\ J_{12} & \Delta\epsilon_2 + \Omega & J_{23} \\ J_{13} & J_{23} & \Delta\epsilon_3 + \Omega \end{pmatrix} \tag{3.7}$$

written as a direct sum of the ground-state block and the one exciton block, according to Eq. (2.11). The two-exciton block is omitted, because we do not use it now. Its presence is however crucial for calculation of nonlinear spectra. Further in this work, we use more specific form of Hamiltonian (3.7), assuming

$$\Delta\epsilon \equiv \Delta\epsilon_2 - \Delta\epsilon_1 = \Delta\epsilon_3 - \Delta\epsilon_2 \,, \tag{3.8a}$$

$$J \equiv J_{12} = J_{13} = J_{23} \,. \tag{3.8b}$$

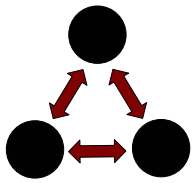

Figure 3.2: Illustration of the trimer structure.

Correlation functions $C_i(t)$ of i-th molecule depend on the bath temperature T, reorganisation energy λ_i and correlation time τ_{C}^i. The local model of correlation functions (2.13) is used, i.e. the fluctuations on different molecules are not correlated. The system

[3]Despite the fact that a trimer is the simplest system where all the effects we are interested in are involved, it is still pretty complicated. Especially number of graphs is big. For this reason we decided to move most of them to Appendix A, although we refer to them from the text of this section.

is excited by a short laser pulse to the state given by (1.78) at $t = 0$. The dipole moment operator

$$\hat{\mu} = \mu_0 \begin{pmatrix} 0 & 1 & 1 & 1 \\ 1 & 0 & 0 & 0 \\ 1 & 0 & 0 & 0 \\ 1 & 0 & 0 & 0 \end{pmatrix} \tag{3.9}$$

is used. Again, only the ground state and the one-exciton block are given. The laser field intensity E_0 from Eq. (1.78) and dipole momentum amplitude μ_0 are chosen to be[4]

$$E_0\mu_0 = 0.4 \text{ cm}^{-1} \text{ fs} \tag{3.11}$$

in the whole work, if not stated otherwise.

In the second order description of the excitation, the two-exciton block is not excited. The population of the ground state is constant after the excitation, so we calculate only the time evolution of the populations of one-excitons and evolution of the optical coherences (OC).

3.4.2 Comparison of the Time Evolution in Various Approximations

We compare the time evolution of the trimer populations and optical coherences solved using the QME, the Markov approximation and secular approximation in this subsection. In appendix A.1, we can see results of three numerical experiments, performed for different electron excitation energy levels, $\Delta\epsilon$, on figures A.1-A.5.

Let us examine the time evolution of the 1-exciton block. On Fig. A.1, we can see that for a homotrimer with $\Delta\epsilon = 0$, the lower excitonic state is twice degenerated. Because of this fact, aggregate is in the excitonic eigenstate after excitation in $t = 0$, therefore difference between the secular approximation and the Markov approximation is very small. (There are no coherences to be neglected in the excitonic basis and the system apparently stays approximately in the excitonic eigenstate.) Fig. A.3a illustrates failure of the Markov approximation (see Section 3.1) – the negative probabilities occur in the thermal equilibrium and the coherences do not disappear. Transforming it into bases where coherences are zero cannot, of course, change negative populations to be positive. From the graphs

[4]There might be certain confusion about the used units, but it can be easily checked that everything is all right. There is a term

$$\frac{E(t)\mu_0}{\hbar} = \frac{E_0\mu_0\delta(t)}{\hbar} \tag{3.10}$$

in the time evolution equation (1.69). This term contributes to the value of the density matrix time derivative, which has dimension of inverse time. $E(t)\mu_0$ has clearly a dimension of energy, therefore because $\delta(t)$ has a dimension of inverse time, E_0, defined by Eq. (1.74), has a dimension of energy multiplied by time. It represents laser electric field intensity integrated over time.

on Figs. A.1f-A.3f, we can see that coherences in the direct solution of the QME do not disappear too. This is discussed in Section 3.3 in detail.

Fig. A.4 shows the time evolution of the optical coherences. One can see very a sharp difference between the Redfield equations and the QME, which predicts an oscillations of the OC envelope.

In Section A.4, we also examine case where the interaction energies λ_i related to the i-th molecule differ from each other. Numerical calculations suggest (Fig. A.13) that difference between molecules interaction energies increases the value of the coherences which remain in limit $t \to \infty$. It also slightly changes the shape of the optical coherences envelope – it adds some characteristic oscillations. (Compare Fig. A.13b and Fig. A.14b with Fig. A.4e.)

We can make an important observation – *coherences in the Markov approximation decay approximately in the same time as in the secular approximation, while in the QME solution, they decay in much longer time.* This is an important result, because it implies that the observed long lasting oscillations in the FMO 2D spectrum [5], can be explained by the QME, but not by the Redfield equations.

3.4.3 Temperature Dependence

Let us examine a temperature dependence of the system time evolution. We take the Hamiltonian of the trimer (3.7) again, and perform calculation based on the QME for multiple temperatures. The result is shown on Fig. A.11. We focus only on the population 1, coherence 12 and optical coherence 2 of the trimer to preserve clarity. The results for other populations and coherences are analogous.

First observation we can make is that the population approaches the thermal equilibrium, which shifts with temperature. The amplitude of oscillations in the beginning of the time evolution increases with temperature, so do their frequency, although there is only a small shift in it. We can make the same observation in case of the one-exciton coherence. Their persisting real part decreases with temperature, which raises the question if the excitonic basis is the one where relaxation takes places at least in high temperature limit.

In the time evolution of the optical coherence, we can see only its envelope – its oscillations are too fast to be reasonably plotted and depend only on properties of $\hat{H}_{\mathrm{S}}$, not of the correlation functions properties (T,λ_i,τ_{C}^i). Frequency of the occurrence of the envelope maxima increases with the temperature much like its amplitude. Numerical result also does not suggest that the optical coherence decay time would be significantly temperature-dependent.

3.4.4 Coherence Transfer Effects, Time Evolution Superoperator

Probably the best way of illustrating coherence transfer effects is to study the components of the time evolution superoperator $\mathcal{U}_{ij,kl}(t)$, which transforms the density operator element $\rho_{\mathrm{S}kl} = \delta_{kl}$ to matrix $\rho_{\mathrm{S}ij}(t)$. (Let indices i, j, k, l, go through 1-exciton states and index g represent ground state in this subsection.)

Elements of $\mathcal{U}_{ij,kl}(t)$, where $k \neq l$, $i \neq j$ and $k \neq i \vee j \neq l$ represent coherence-coherence[5] transfer, elements $k \neq l$, $i = j$ represent contribution from coherence to population, elements $k = l$, $i = j$ from population to population and elements $k = l$, $i \neq j$ contribution from population to coherence. Elements $\mathcal{U}_{gj,gl}(t)$ are related to optical coherences. Case $j = l$ represent OC dephasing, while case $j \neq l$ represent OC-OC transfer.

In the appendix A.2, $\mathcal{U}$ is calculated for the trimer for energy differences $\Delta\epsilon = 20$ and $\Delta\epsilon = 120$, using the QME. Generally, we can say that all components of the type coherence $\rightarrow$ populations and coherence $\rightarrow$ coherences disappear in sufficiently long time, while components of the type population $\rightarrow$ populations do not relax exactly to the canonical equilibrium, therefore even terms population $\rightarrow$ coherences do not disappear in long times. However, only the real part of the coherences remains in the excitonic basis. Further, coherences survive much longer time than the coherence time τ_{C}^{i} used in correlation functions. This effect can be attributed to the sensitivity of the QME to whole system history.

Optical coherences (Fig. A.8) exhibit fast oscillations because of the large energy difference between ground state and one-exciton block. They depend on the Hamiltonian $\hat{H}_{\mathrm{S}}$, in particular on value of optical frequency Ω, and not on much slower relaxation process described by correlation function properties. From these reasons we can focus only on slowly changing envelope of these oscillations.

[5]Here, by word coherence, we understand in particular the coherence inside the 1-exciton block, i.e. not the optical coherences.

Chapter 4

Conclusion

We modelled numerically the time evolution superoperators for molecular aggregates, considering the one-exciton states[1], in the Markov and secular approximations and the convolutional QME with no additional approximation. Comparing them, we can conclude that the Markov approximation does not give correct results for wide range of parameters nor can it explain long-lasting oscillations of the coherences visible in the FMO 2D spectra. The secular approximation, which completely neglects coherence transfer effects, is numerically more stable than the Markov approximation and leads to canonical thermal equilibrium. The QME itself predicts long-lasting coherences oscillations, most probably because the system time evolution is given by its whole history (damped by the correlation function), not only by its actual state. They may be caused by oscillations of coherences in the one-exciton block, i.e. by the coherence transfer effects. This means that the Redfield equations cannot explain the long-lasting coherences oscillations observed on the FMO complex while the QME can.

It have been observed and discussed on the basis of numerical calculations, that the exciton basis is generally not the one in which the relaxation to the thermal equilibrium takes place. This effect, again, cannot be explained by the secular approximation.

The temperature dependence of the trimer time evolution has been examined and it has been observed that the amplitude of the populations oscillations increases with temperature in our model, coherence decay time does not change significantly and the frequency of the optical coherence envelope maxima, as well as frequency of the populations oscillations, increases.

The amplitude of the coherence-transfer effects has been discussed on an example of a trimer. The value of the coherence-coherence terms is approximately one order of magnitude smaller than the value of coherence itself and it cannot be generally neglected. They contribute to coherences and population oscillations and they last approximately the same time as the coherences themselves. The coherence transfer cannot be separated from a contribution of the QME convolution terms, therefore it cannot be said, that presence of one coherence contributes to change of a second coherence. Only the components of the

[1] However, we described also the theory for the two-exciton states and our program is written to use them as well.

time evolution superoperator can be calculated – they were calculated in the Subsection 3.4.4 and the related appendix A.2.

The obtained results indicate that there are aspects of the problem that cannot be satisfactorily described by the Redfield equations and the QME without the Markov and secular approximations has to be solved directly instead. The obtained evolution superoperators can be used to calculate 2D spectra of molecular aggregates in order to get a direct comparison with experiment. This is also a course of the planned future work on this field.

Appendix A

Supplementary Graphs

Here, we present all graphs which would clutter the previous chapters.

In all sections of this appendix, except of the section A.2, following notation holds: population 1, coherence 12 and OC 1 are blue, population 2, coherence 13 and OC 2 are purple and population 3, coherence 23 and OC 3 are yellow. In section A.3, different colours denote different temperatures specified in the figure description. Temperature ordering from the lowest to the highest can be easily assigned according to thermal equilibria of populations.

We also remind that populations in the 1-exciton block are not normalized to unity – the initial condition is given by a laser ultra-short pulse of a chosen intensity, therefore there is also some occupancy of the ground state, whose time evolution is trivial and not plotted. In the section A.2, on the other hand, components of time evolution superoperator are plotted directly, and normalisation of populations to unity holds.

A.1 Comparison of Evaluation Methods, Trimer

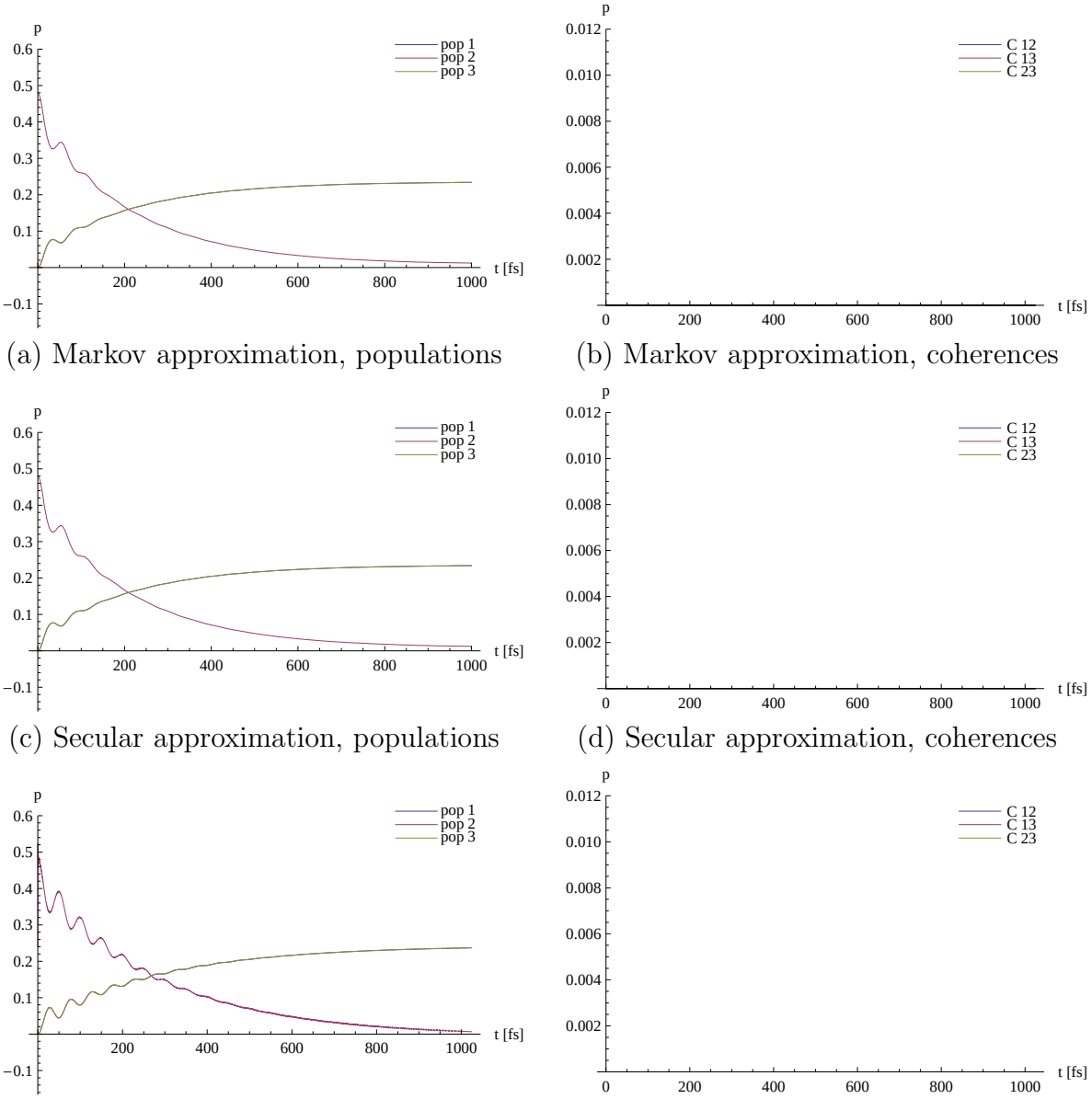

(a) Markov approximation, populations

(b) Markov approximation, coherences

(c) Secular approximation, populations

(d) Secular approximation, coherences

(e) QME, populations

(f) QME, coherences

Figure A.1: Populations of the trimer.
$\Delta\epsilon = 0\ \mathrm{cm}^{-1}, J = 200\ \mathrm{cm}^{-1}, \tau_{\mathrm{C}}^{i} = 100\ \mathrm{fs}, \lambda_i = 100\ \mathrm{cm}^{-1}, T = 300\ \mathrm{K}$.

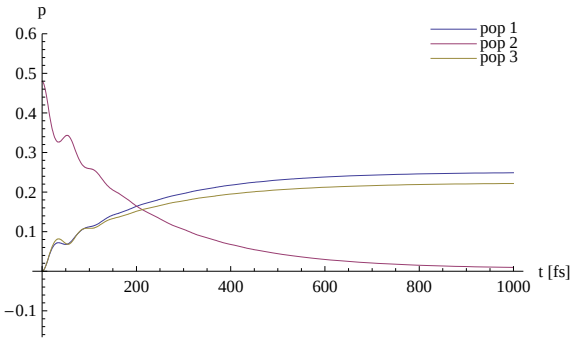

(a) Markov approximation, populations

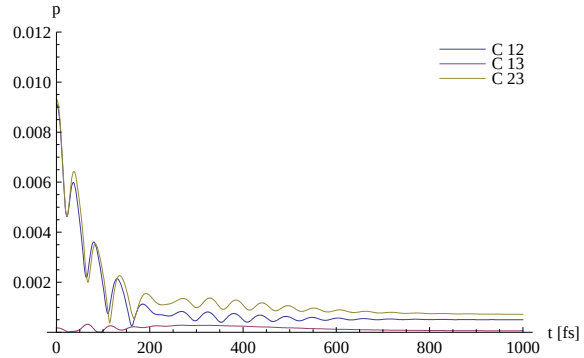

(b) Markov approximation, coherences, Abs x.

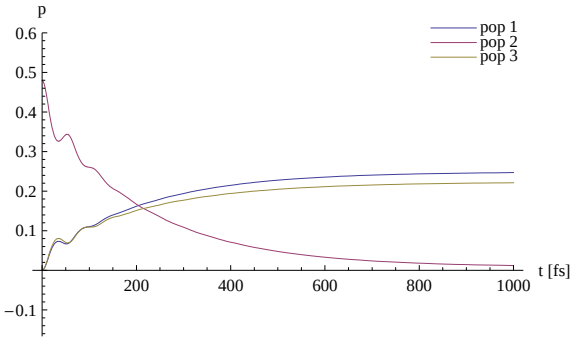

(c) Secular approximation, populations

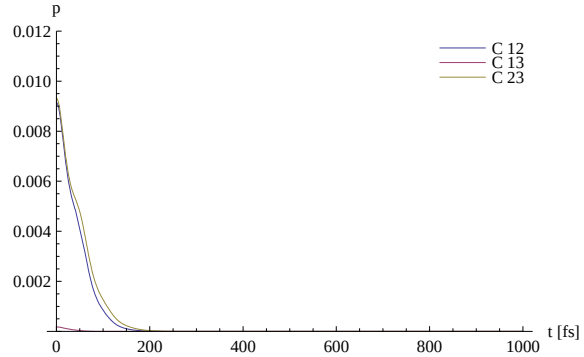

(d) Secular approximation, coherences, Abs x.

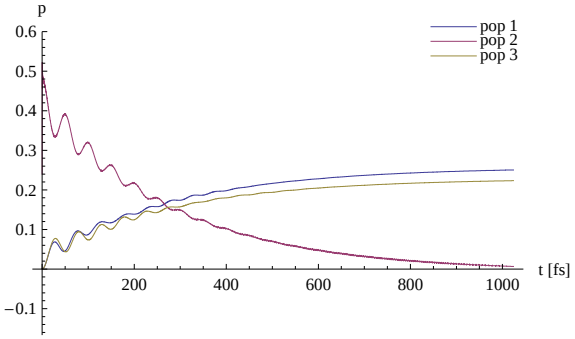

(e) QME, populations

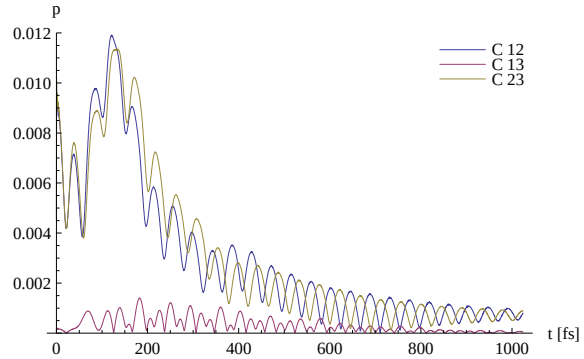

(f) QME, coherences, Abs x.

Figure A.2: Populations of the trimer.
$\Delta\epsilon = 20\ \mathrm{cm}^{-1}, J = 200\ \mathrm{cm}^{-1}, \tau_{\mathrm{C}}^{i} = 100\ \mathrm{fs}, \lambda_i = 100\ \mathrm{cm}^{-1}, T = 300\ \mathrm{K}$.

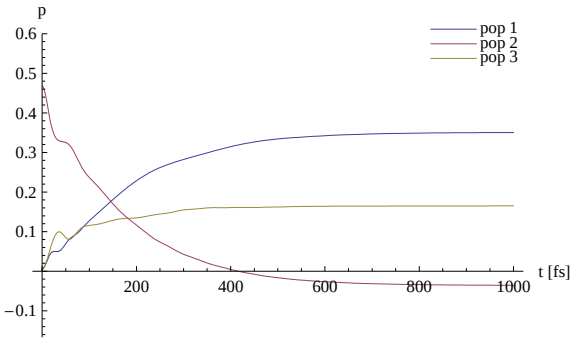

(a) Markov approximation, populations

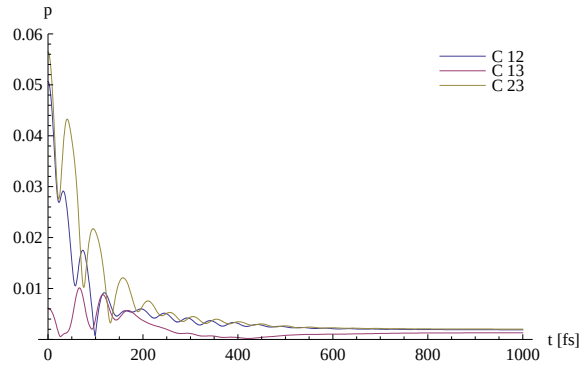

(b) Markov approximation, coherences, Abs x.

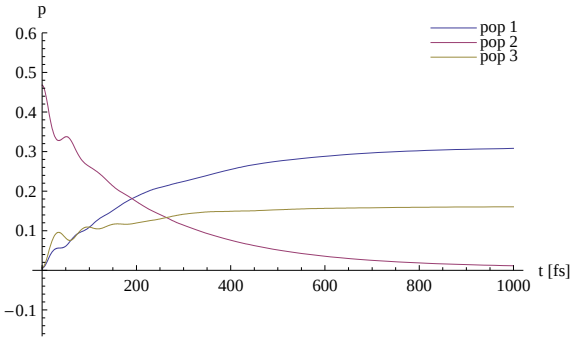

(c) Secular approximation, populations

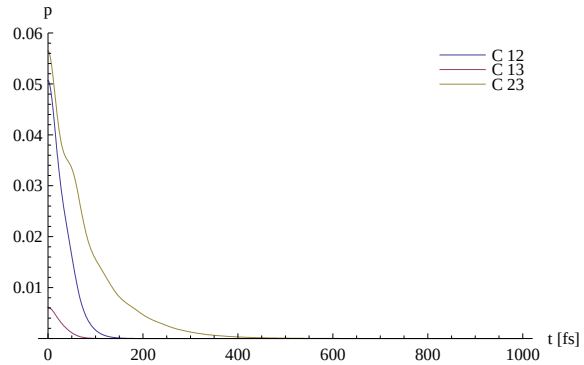

(d) Secular approximation, coherences, Abs x.

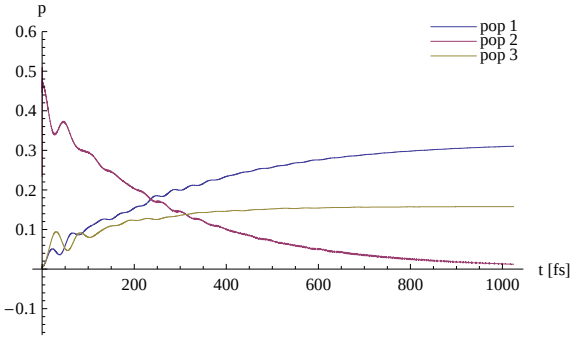

(e) QME, populations

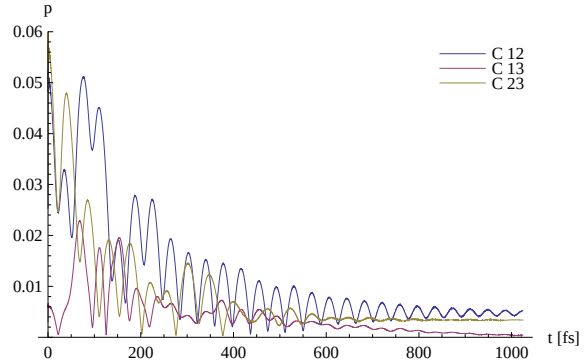

(f) QME, coherences, Abs x.

Figure A.3: Populations of the trimer.
$\Delta\epsilon = 120\ \mathrm{cm}^{-1}$, $J = 200\ \mathrm{cm}^{-1}$, $\tau_{\mathrm{C}}^{i} = 100$ fs, $\lambda_i = 100\ \mathrm{cm}^{-1}$, $T = 300$ K.

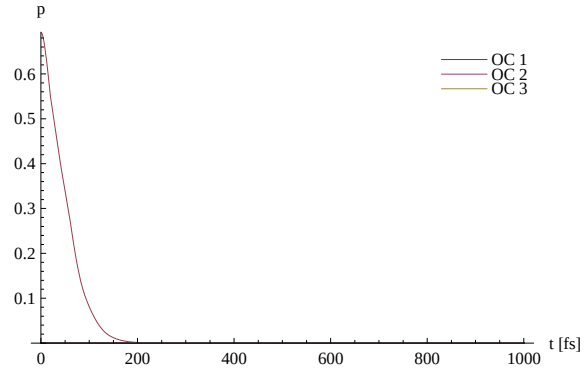

(a) Markov approximation, $\Delta\epsilon = 0$ cm^{-1}.

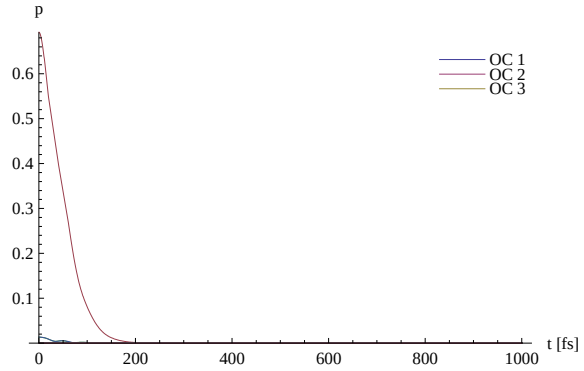

(b) Markov approximation, $\Delta\epsilon = 20$ cm^{-1}.

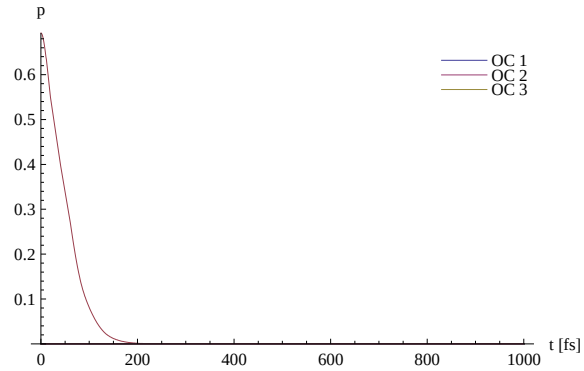

(c) Secular approximation, $\Delta\epsilon = 0$ cm^{-1}.

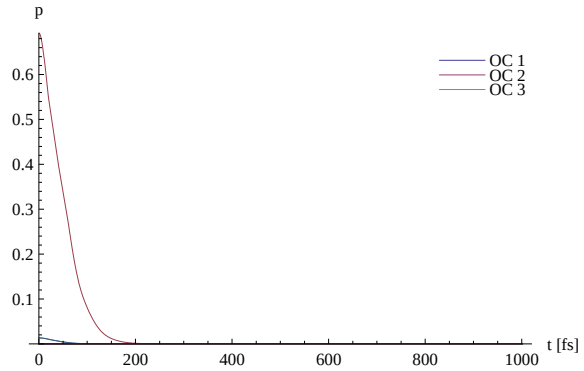

(d) Secular approximation, $\Delta\epsilon = 20$ cm^{-1}.

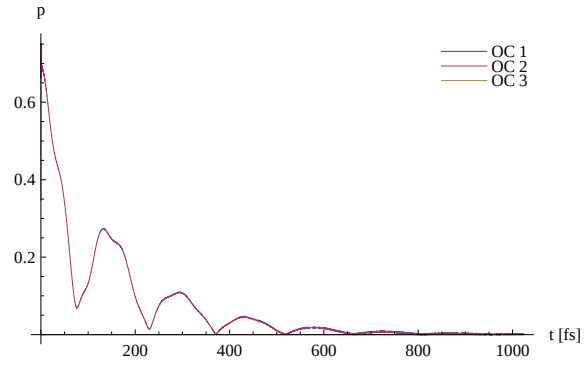

(e) QME, $\Delta\epsilon = 0$ cm^{-1}.

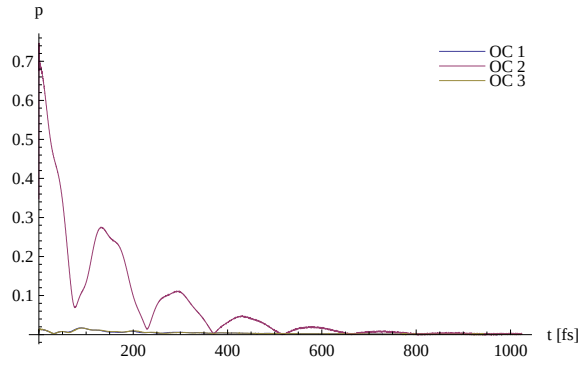

(f) QME, $\Delta\epsilon = 20$ cm^{-1}.

Figure A.4: Optical coherences of the trimer, Abs x.
$\Omega = 10^4$ cm^{-1}, $J = 200$ cm^{-1}, $\tau_{\mathrm{C}}^i = 100$ fs, $\lambda_i = 100$ cm^{-1}, $T = 300$ K.

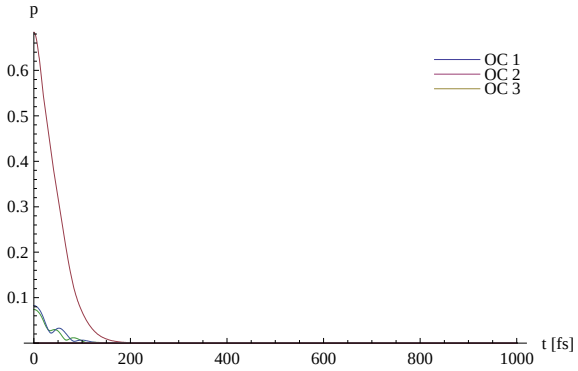

(a) Markov approximation, $\Delta\epsilon = 120$ cm^{-1}.

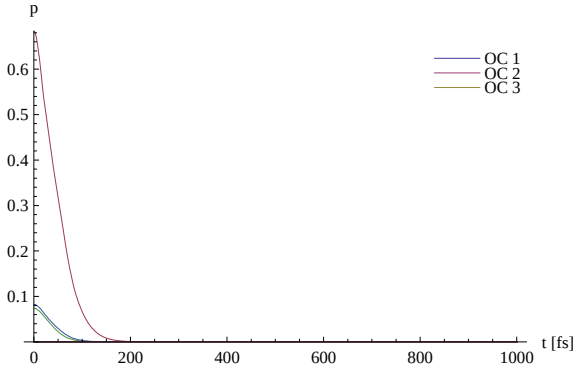

(b) Secular approximation, $\Delta\epsilon = 120$ cm^{-1}.

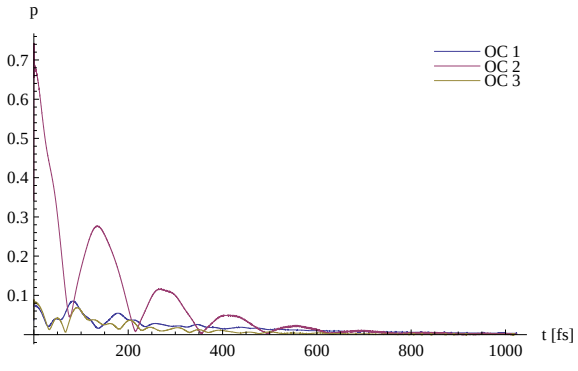

(c) QME, $\Delta\epsilon = 120$ cm^{-1}.

Figure A.5: Optical coherences of the trimer, Abs x.
$\Omega = 10^4$ cm^{-1}, $J = 200$ cm^{-1}, $\tau_{\mathrm{C}}^i = 100$ fs, $\lambda_i = 100$ cm^{-1}, $T = 300$ K.

A.2 Trimer Time-Evolution Superoperator

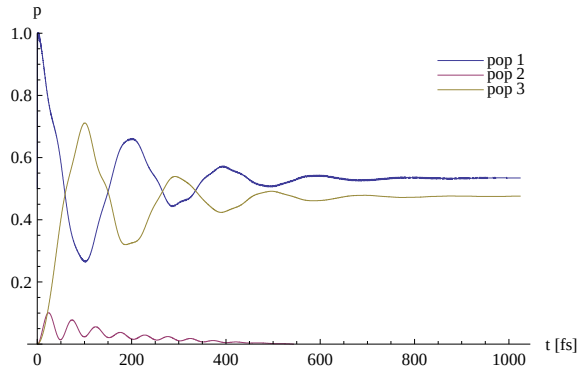

(a) population 1 → populations.

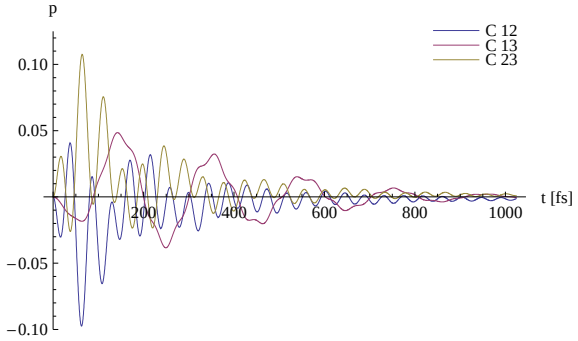

(b) population 1 → coherences, Re x.

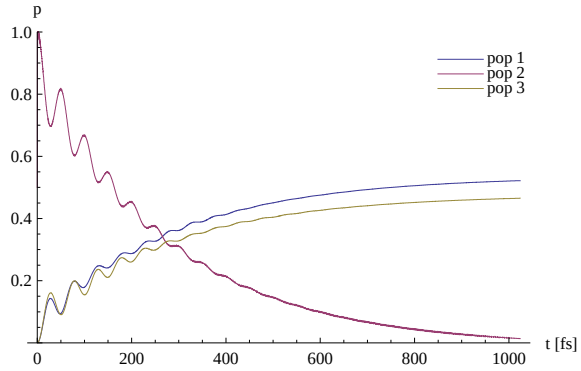

(c) population 2 → populations.

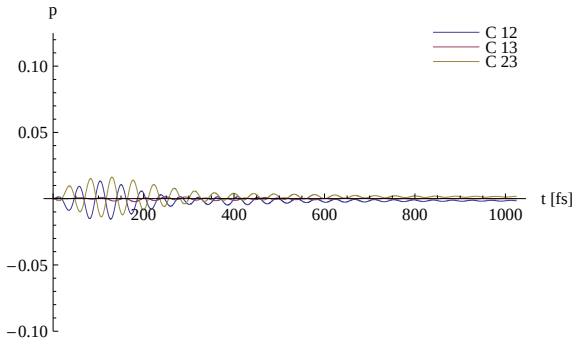

(d) population 2 → coherences, Re x.

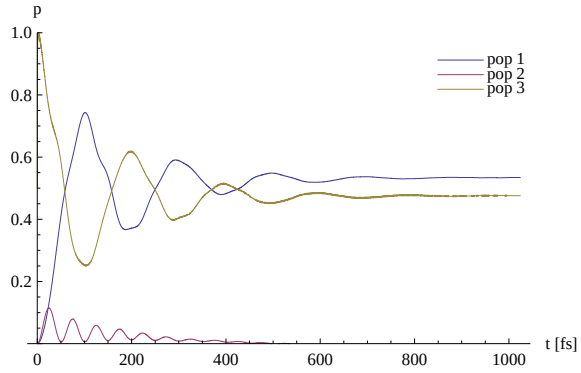

(e) population 3 → populations.

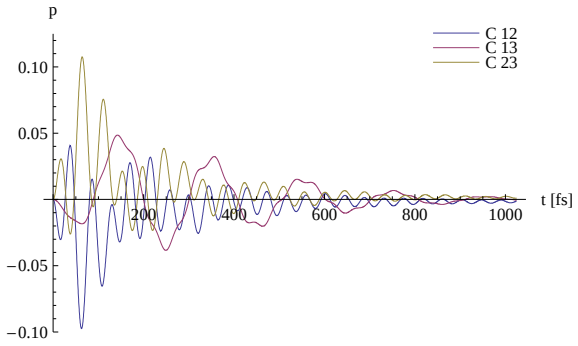

(f) population 3 → coherences, Re x.

Figure A.6: $\mathcal{U}_{ij,kl}(t)$, components: populations → populations & coherences. $\Delta\epsilon = 20\ \mathrm{cm}^{-1}, J = 200\ \mathrm{cm}^{-1}, \tau_{\mathrm{C}}^{i} = 100\ \mathrm{fs}, \lambda_i = 100\ \mathrm{cm}^{-1}, T = 300\ \mathrm{K}$.

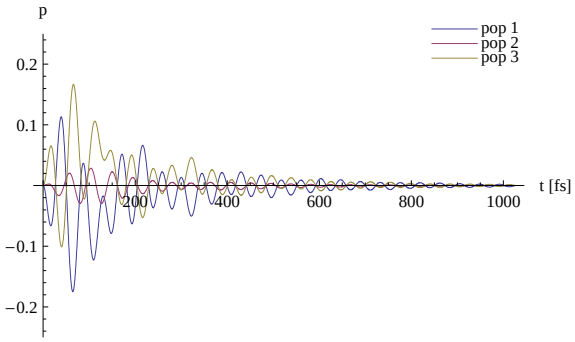

(a) coherence 12 → populations.

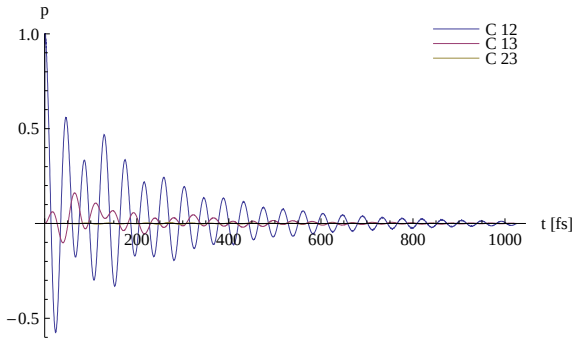

(b) coherence 12 → coherences, $\mathrm{Re}\, x$.

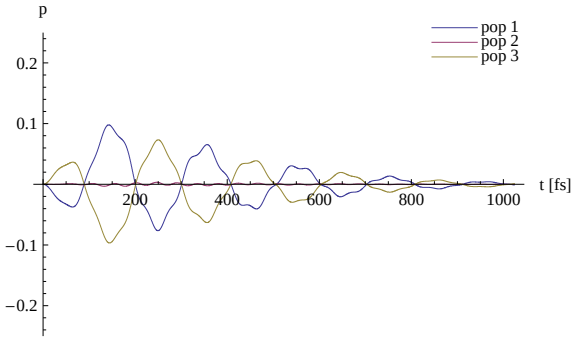

(c) coherence 13 → populations.

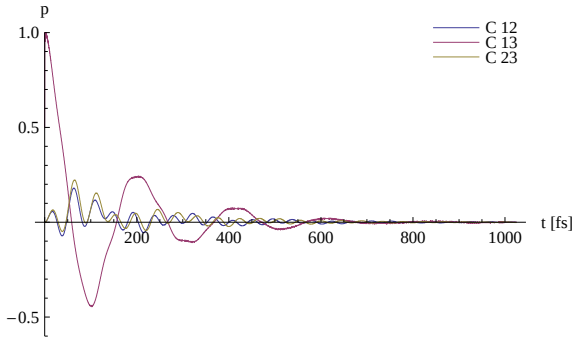

(d) coherence 13 → coherences, $\mathrm{Re}\, x$.

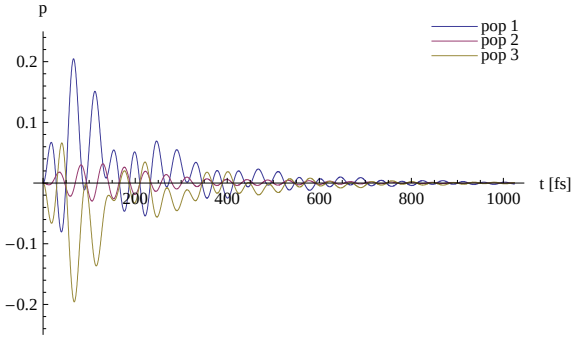

(e) coherence 23 → populations.

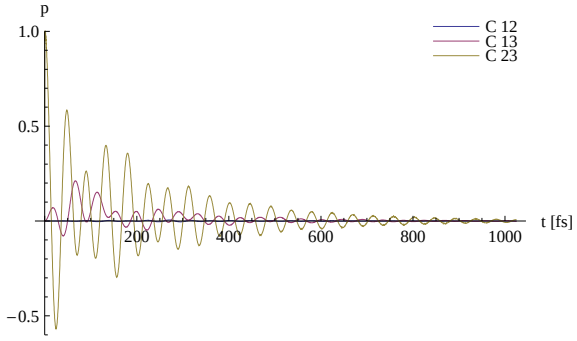

(f) coherence 23 → coherences, $\mathrm{Re}\, x$.

Figure A.7: $\mathcal{U}_{ij,kl}(t)$, components: coherences → populations & coherences. $\Delta\epsilon = 20\ \mathrm{cm}^{-1}, J = 200\ \mathrm{cm}^{-1}, \tau_{\mathrm{C}}^{i} = 100\ \mathrm{fs}, \lambda_i = 100\ \mathrm{cm}^{-1}, T = 300\ \mathrm{K}$.

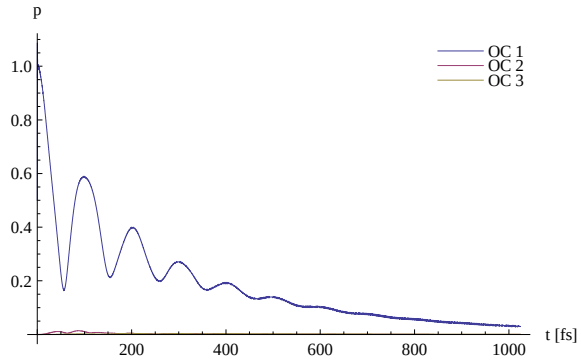

(a) OC 1 → OCs , $\Delta\epsilon = 20$ cm^{-1}, Abs x.

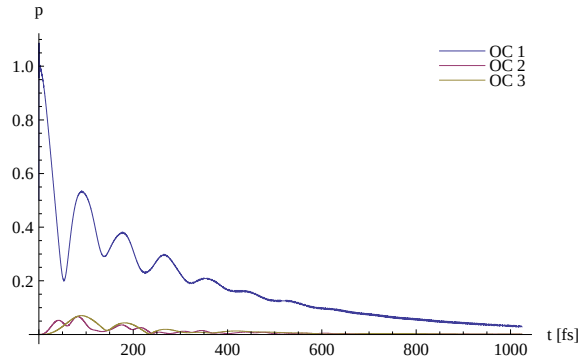

(b) OC 1 → OCs, $\Delta\epsilon = 120$ cm^{-1}, Abs x.

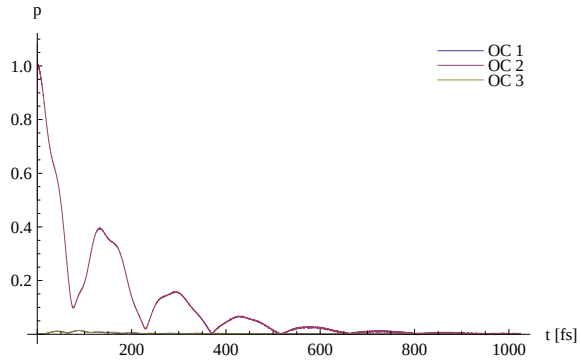

(c) OC 2 → OCs , $\Delta\epsilon = 20$ cm^{-1}, Abs x.

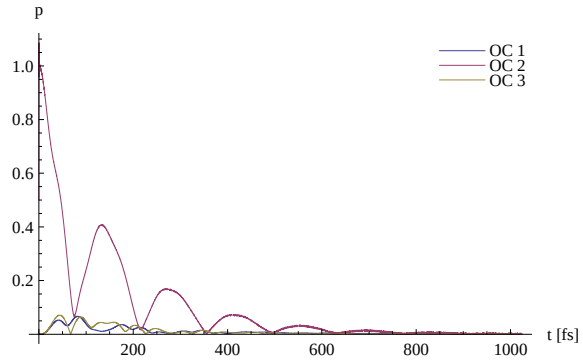

(d) OC 2 → OCs, $\Delta\epsilon = 120$ cm^{-1}, Abs x.

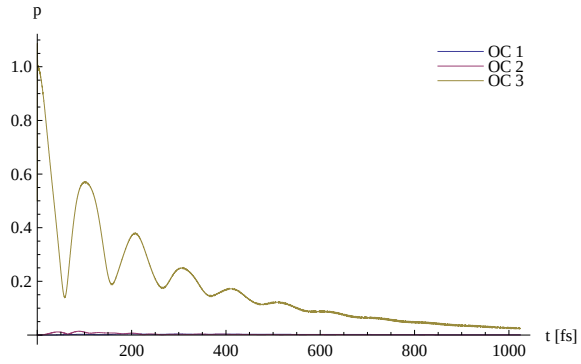

(e) OC 3 → OCs , $\Delta\epsilon = 20$ cm^{-1}, Abs x.

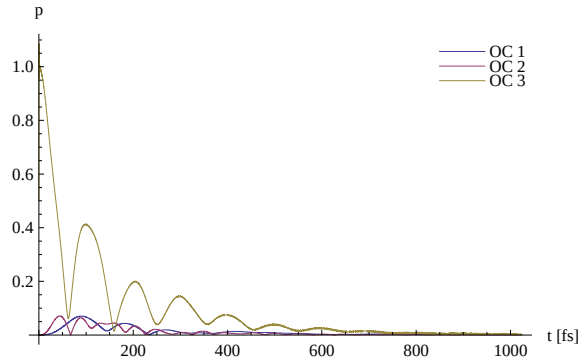

(f) OC 3 → OCs, $\Delta\epsilon = 120$ cm^{-1}, Abs x.

Figure A.8: $\mathcal{U}_{gj,gl}(t)$, components: optical coherences → optical coherences. $\Omega = 10^4$ cm^{-1}, $J = 200$ cm^{-1}, $\tau_C^i = 100$ fs, $\lambda_i = 100$ cm^{-1}, $T = 300$ K.

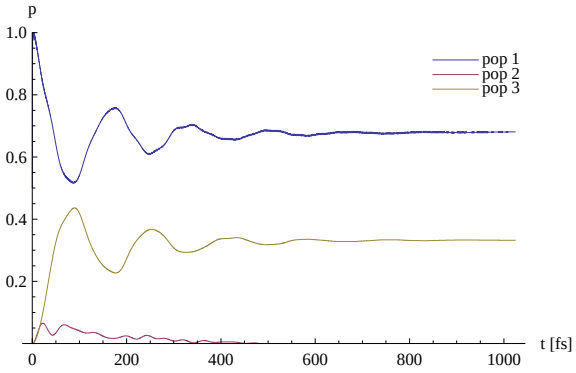

(a) population 1 → populations.

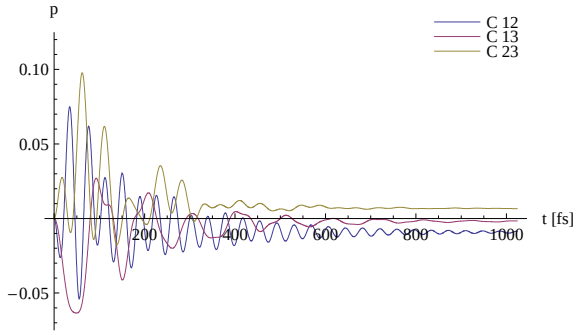

(b) population 1 → coherences, Re x.

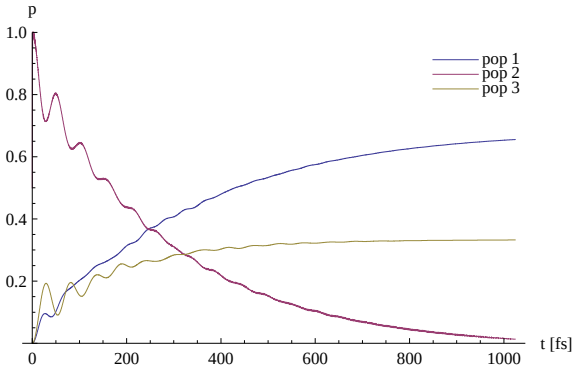

(c) population 2 → populations.

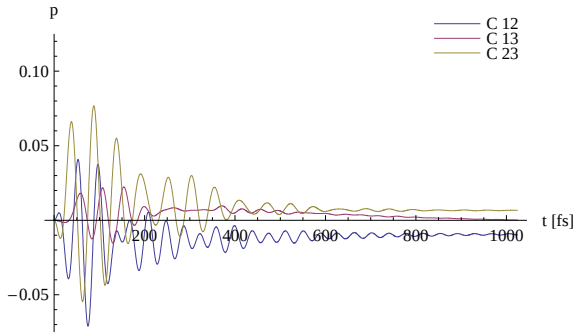

(d) population 2 → coherences, Re x.

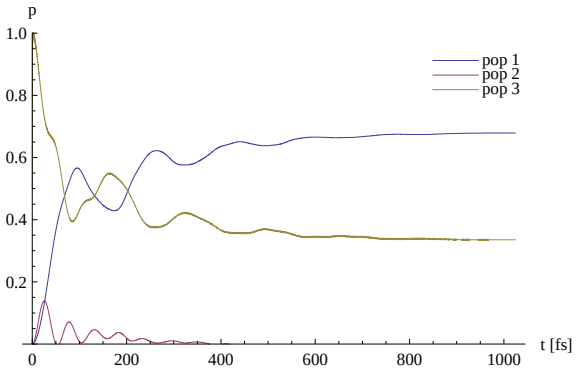

(e) population 3 → populations.

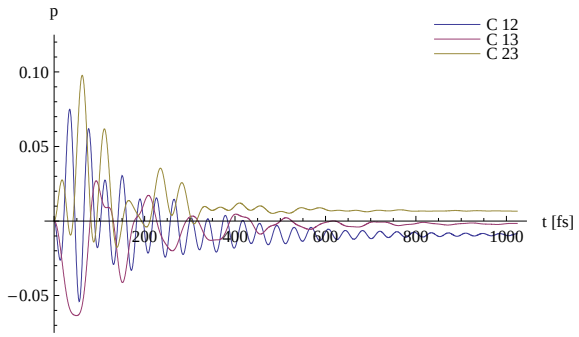

(f) population 3 → coherences, Re x.

Figure A.9: $\mathcal{U}_{ij,kl}(t)$, components: populations → populations & coherences. $\Delta\epsilon = 120\ \mathrm{cm}^{-1}$, $J = 200\ \mathrm{cm}^{-1}$, $\tau_{\mathrm{C}}^{i} = 100$ fs, $\lambda_i = 100\ \mathrm{cm}^{-1}$, $T = 300$ K.

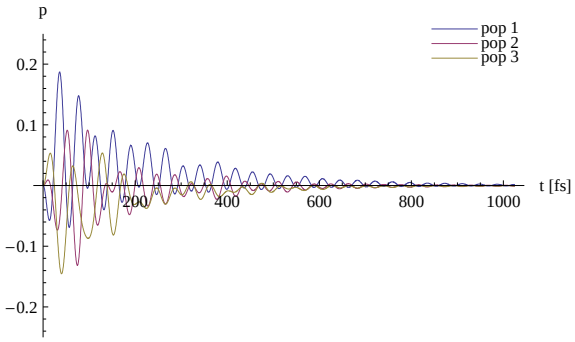

(a) coherence 12 → populations.

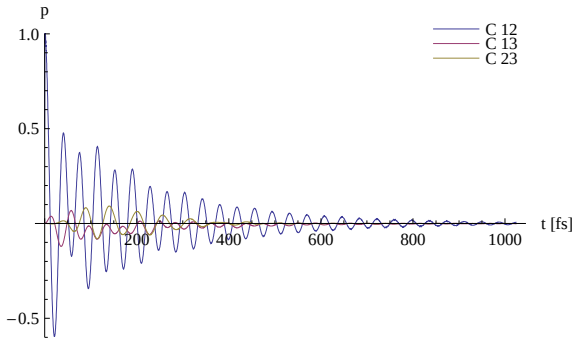

(b) coherence 12 → coherences, $\mathrm{Re}\, x$.

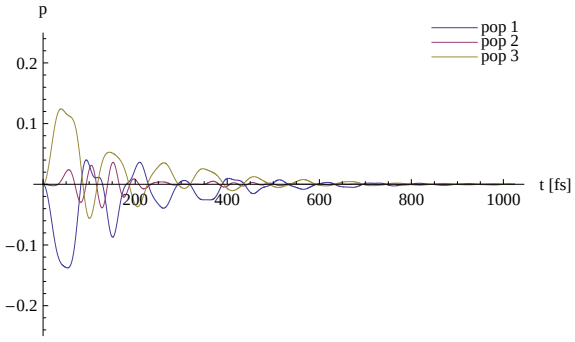

(c) coherence 13 → populations.

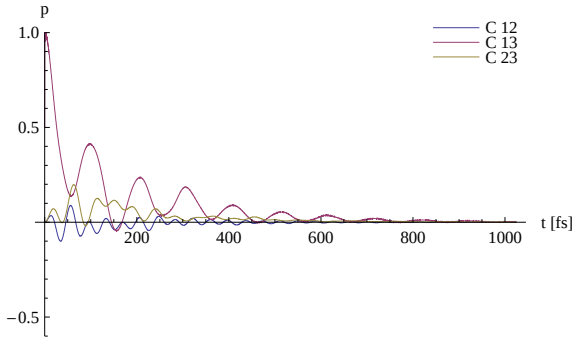

(d) coherence 13 → coherences, $\mathrm{Re}\, x$.

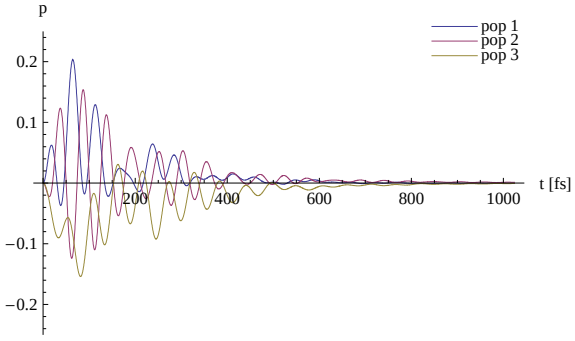

(e) coherence 23 → populations.

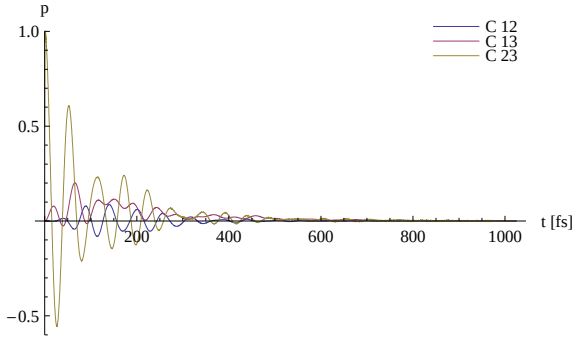

(f) coherence 23 → coherences, $\mathrm{Re}\, x$.

Figure A.10: $\mathcal{U}_{ij,kl}(t)$, components: coherences → populations & coherences. $\Delta\epsilon = 120\ \mathrm{cm}^{-1}$, $J = 200\ \mathrm{cm}^{-1}$, $\tau_{\mathrm{C}}^{i} = 100\ \mathrm{fs}$, $\lambda_i = 100\ \mathrm{cm}^{-1}$, $T = 300\ \mathrm{K}$.

A.3 Temperature Dependence, Trimer

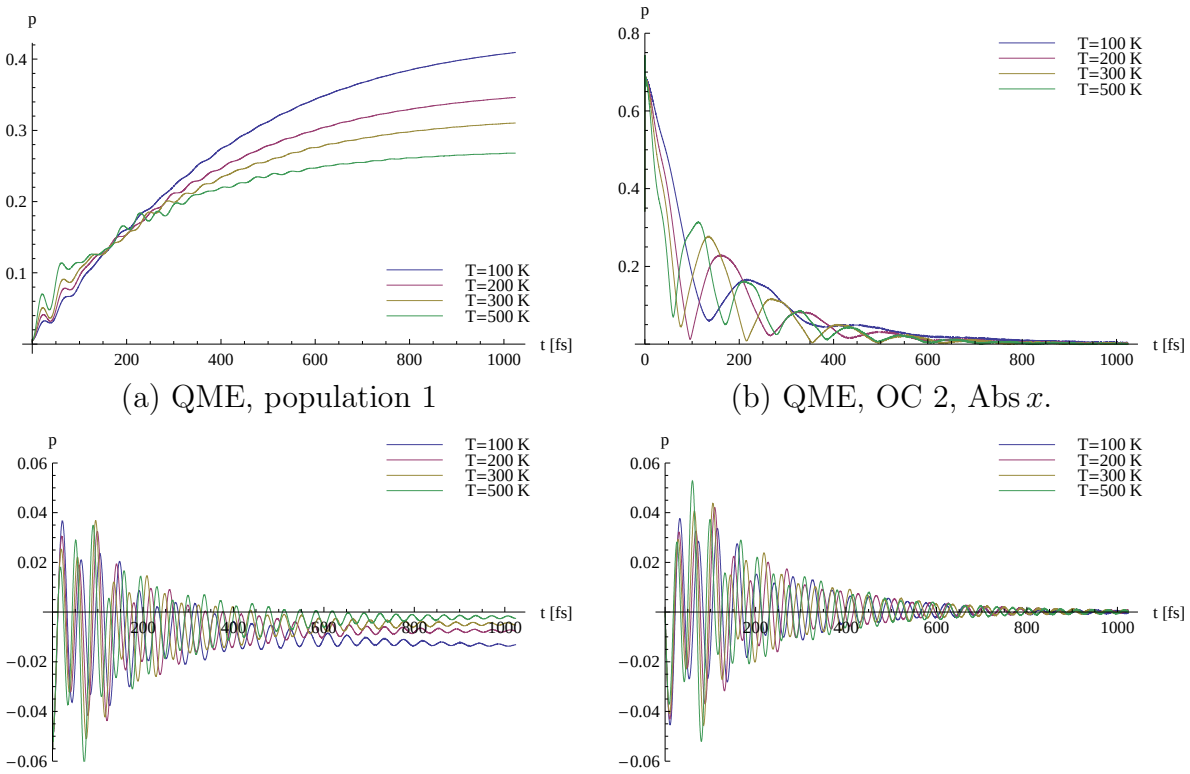

(a) QME, population 1

(b) QME, OC 2, Abs x.

(c) QME, coherence 12, Re x

(d) QME, coherence 12, Im x.

Figure A.11: T dependence of selected trimer population and coherence time evolution. $\Delta\epsilon = 120\ \mathrm{cm}^{-1}, J = 200\ \mathrm{cm}^{-1}, \Omega = 10^4\ \mathrm{cm}^{-1}, \tau_{\mathrm{C}}^i = 100\ \mathrm{fs}, \lambda_i = 100\ \mathrm{cm}^{-1}$, $T = 100\ \mathrm{K}, 200\ \mathrm{K}, 300\ \mathrm{K}$ & $500\ \mathrm{K}$.

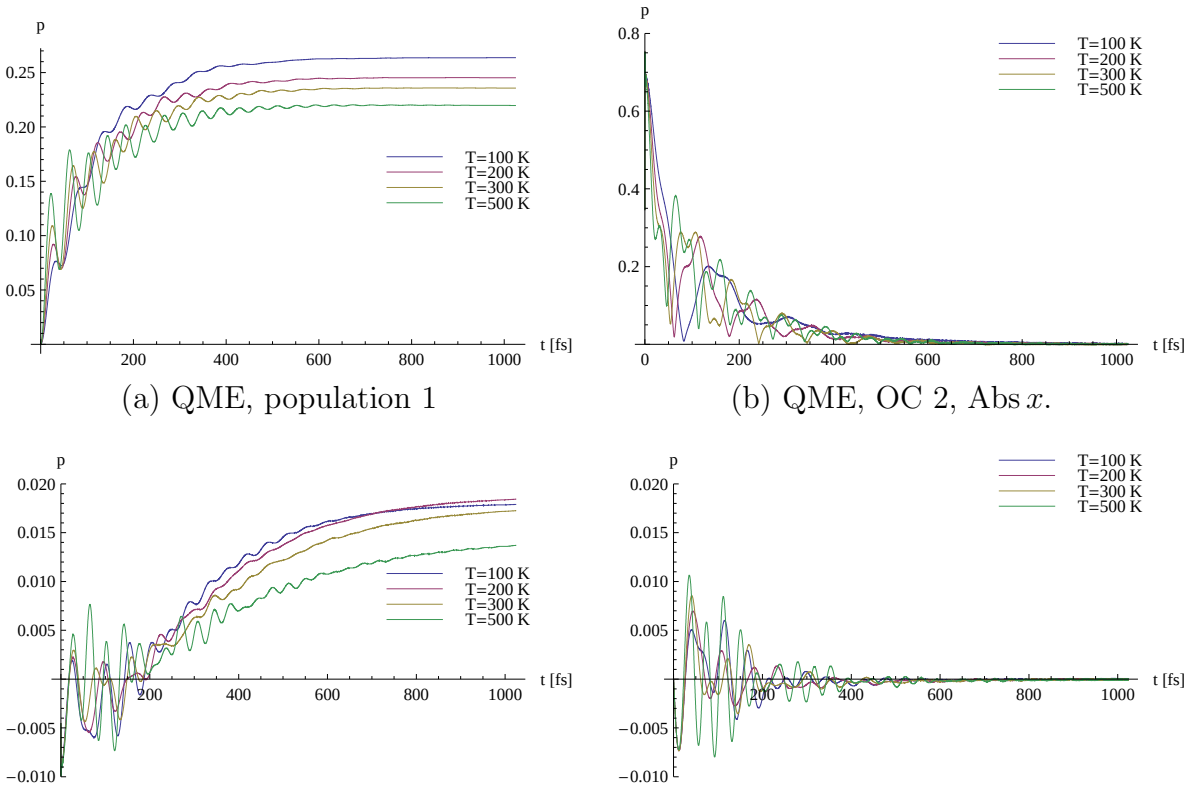

(a) QME, population 1

(b) QME, OC 2, Abs x.

(c) QME, coherence 12, Re x

(d) QME, coherence 12, Im x.

Figure A.12: T dependence of selected trimer population and coherence time evolution. $\Delta\epsilon = 20\ \mathrm{cm}^{-1}, J = 200\ \mathrm{cm}^{-1}, \Omega = 10^4\ \mathrm{cm}^{-1}, \tau_{\mathrm{C}}^{i} = 100\ \mathrm{fs}, \lambda_i = 100 + 60i\ \mathrm{cm}^{-1}$, $T = 100\ \mathrm{K}, 200\ \mathrm{K}, 300\ \mathrm{K}\ \&\ 500\ \mathrm{K}$.

A.4 Trimer Time Evolution for Another Interesting Cases

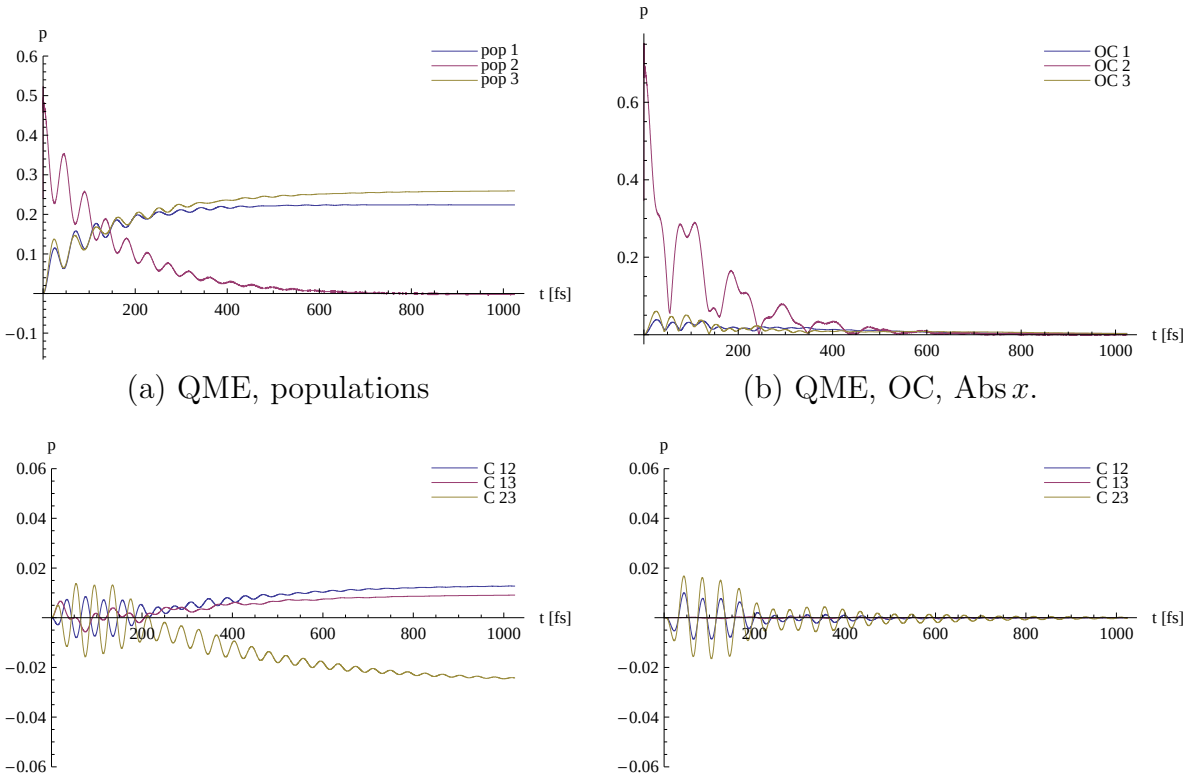

(a) QME, populations

(b) QME, OC, Abs x.

(c) QME, coherences, Re x

(d) QME, coherences, Im x.

Figure A.13: Trimer time evolution with different reorganisation energies on its molecules. $\Delta\epsilon = 0$ cm^{-1}, $J = 200$ cm^{-1}, , $\Omega = 10^4$ cm^{-1}, $\tau_{\mathrm{C}}^i = 100$ fs, $\lambda_i = 100 + 60i$ cm^{-1}, $T = 300$ K.

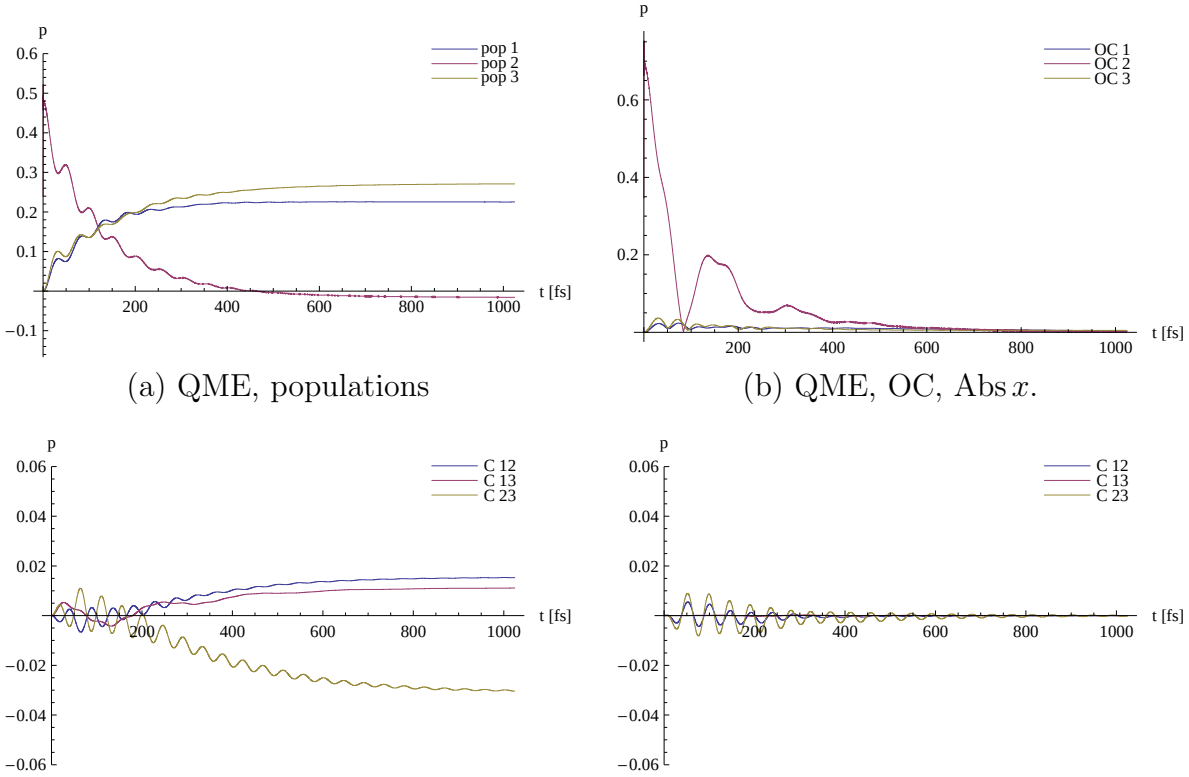

(a) QME, populations

(b) QME, OC, Abs x.

(c) QME, coherences, Re x

(d) QME, coherences, Im x.

Figure A.14: Trimer time evolution with different reorganisation energies on its molecules. $\Delta\epsilon = 0\ \mathrm{cm}^{-1}, J = 200\ \mathrm{cm}^{-1}, \Omega = 10^4\ \mathrm{cm}^{-1}, \tau_{\mathrm{C}}^i = 100\ \mathrm{fs}, \lambda_i = 100 + 60i\ \mathrm{cm}^{-1}, T = 100\ \mathrm{K}$.

Bibliography

[1] Blankenship R. E., Miller M., Olson J. M.: *Antenna Complexes from Green Photosynthetic Bacteria*, chapter of book Anoxygenic Photosynthetic Bacteria, Springer Netherlands, ISBN 978-0-7923-3681-5,(2004), pp. 399-435, Vol 2; doi:10.1007/0-306-47954-0

[2] Jonas D.M.: *Two-dimensional femtosecond spectroscopy*, Annu. Rev. Phys. Chem. 2003. 54:425–63; Doi:10.1146/annurev.physchem.54.011002.103907

[3] Chernyak V., Mukamel S.: *Collective coordinates for nuclear spectral densities in energy transfer and femtosecond spectroscopy of molecular aggregates*, J. Chem. Phys. 105, 4565 (1996), Doi:10.1063/1.472302

[4] Kwa S. L. S., Van Amerongen H., Su Lin, Dekker J. P., Van Grondelle R., Struve W. S.: *Ultrafast energy transfer in LHC-II trimers from the Chl a/b light-harvesting antenna of photosystem II*, Biochimica et biophysica acta. Bioenergetics ISSN 0005-2728, 1992, vol. 1102, no°2, pp. 202-212 (24 ref.)

[5] Engel G.S., Calhoun T.R., Read E.L., Ahn T.K., Mančal T., Cheng Y.C., Blankenship R.E., Fleming G.R.: *Evidence for wavelike energy transfer through quantum coherence in photosynthetic systems*, Nature 2007 Apr 12; 446(7137):782-6; Doi:10.1038/nature05678

[6] Kühn O., May V.: *Charge and Energy Transfer Dynamics in Molecular Systems*, WILEY-VCH Verlag GmbH & Co.KGaA, 2004; Doi:10.1002/9783527602575.fmatter

[7] Fain B.: *Irreversibilities in Quantum Mechanics*, Kluwer Academic Publishers, 2000; doi:10.1007/0-306-47128-0

[8] Novoderezhkin V., Wendling M., van Grondelle R.: *Intra- and Interband Transfers in the B800-B850 Antenna of Rhodospirillum molischianum: Redfield Theory Modeling of Polarized Pump-Probe Kinetics*, J. Phys. Chem. B, 2003, 107 (41), 11534-11548; DOI:10.1021/jp035432l

[9] Zigmantas D., Read E. L., Mančal T., Brixner T., Gardiner A. T., Cogdell R. J., Fleming G. R.: *Two-dimensional electronic spectroscopy of the B800–B820 light-harvesting complex*, PNAS 2006, 103, 12672-12677, doi:10.1073/pnas.0602961103

[10] Barvík I., Čápek V., Heřman P.: *Towards proper parametrization in the exciton transfer and relaxation problem*, Journal of Luminescence 83-84 (1999) 105-108; Doi:10.1016/S0022-2313(99)00081-2

[11] Mukamel S.: *Principles of Nonlinear Optical Spectroscopy*, Oxford University Press, 1995.

[12] Hänggi P., Ingold G.L.: *Fundamental Aspects of Quantum Brownian Motion*, Chaos 15, 026105 (2005); Doi:10.1063/1.1853631

[13] Geva E., Rosenman E., Tannor D. *On the second-order corrections to the canonical equilibrium density matrix*, J. Chem. Phys. 113, 1380 (2000); doi:10.1063/1.481928

[14] Press W. H., Teukolsky S. A., Vetterling W. T., Flannery B. P. *Numerical Recipes in Fortran 90:The Art of Scienfic Computing*, Cambridge University Press, 1996, DOI: 10.1021/ja965936f

[15] Wolfram S et al.: *Wolfram Mathematica® Documentation Center*, Wolfram Inc., 2009, http://reference.wolfram.com/mathematica/guide/Mathematica.html

[16] Mančal T., Valkunas L., Fleming R.: *Theory of exciton–charge transfer state coupled systems*, Chemical Physics Letters 432, (2006), 301–305, Doi:10.1016/j.cplett.2006.10.055

[17] Meier C., Tannor D. J.: *Non-Markovian evolution of the density operator in the presence of strong laser fields*, J. Chem. Phys. 111, 3365 (1999); Doi:10.1063/1.479669